

The Carina Nebula: A Laboratory for Feedback and Triggered Star Formation

Nathan Smith

Astronomy Department, University of California, 601 Campbell Hall, Berkeley, CA 94720, USA

Kate J. Brooks

ATNF, P.O. Box 76, Epping NSW 1710, Australia

Abstract. The Carina Nebula (NGC 3372) is our richest nearby laboratory in which to study feedback through UV radiation and stellar winds from very massive stars during the formation of an OB association, at an early phase before supernova explosions have disrupted the environment. This feedback is triggering new generations of star formation around the periphery of the nebula, while simultaneously evaporating the gas and dust reservoirs out of which young stars are trying to accrete. Carina is currently powered by UV radiation from 65 O-type stars and 3 WNH stars, but for most of its lifetime when its most massive star (η Carinae) was on the main-sequence, the Carina Nebula was powered by 70 O-type stars that produced a hydrogen ionizing luminosity 150 times stronger than in the Orion Nebula. At a distance of 2.3 kpc, Carina has the most extreme stellar population within a few kpc of the Sun, and suffers little interstellar extinction. It is our best bridge between the detailed star-formation processes that can be studied in nearby regions like Orion, and much more extreme but also more distant regions like 30 Doradus. Existing observations have only begun to tap the tremendous potential of this region for understanding the importance of feedback in star formation — it will provide a reservoir of new discoveries for the next generation of large ground-based telescopes, space telescopes, and large submillimeter and radio arrays.

1. Introduction

Feedback from young massive stars may play an integral role in star and planet formation. Most stars are born in OB associations (Blaauw 1964; Lada & Lada 2003), in the vicinity of hot massive stars spawned only from giant molecular clouds. The effects of feedback from these massive stars cannot be studied in nearby quiescent regions of star formation.

The Carina Nebula (Fig. 1; NGC 3372) is the southern hemisphere's largest and highest surface brightness nebula — some central parts of the nebula are even brighter than the Orion Nebula. It provides an ideal laboratory in which to study ongoing star formation in the vicinity of some of the most massive stars known, including our Galaxy's most luminous known star, η Carinae. Carina's star clusters are not as densely packed as those of 30 Dor in the LMC (Massey & Hunter 1998), or objects in our own Galaxy like the Arches cluster near the Galactic center (Najarro et al. 2004; Figer et al. 1999, 2002), NGC 3603 (Moffat et al. 2002), or W49 (Welch et al. 1987). However, these other regions are too distant for detailed studies of small-scale phenomena like irradiated protoplanetary disks and jets, and their study is hampered by considerably

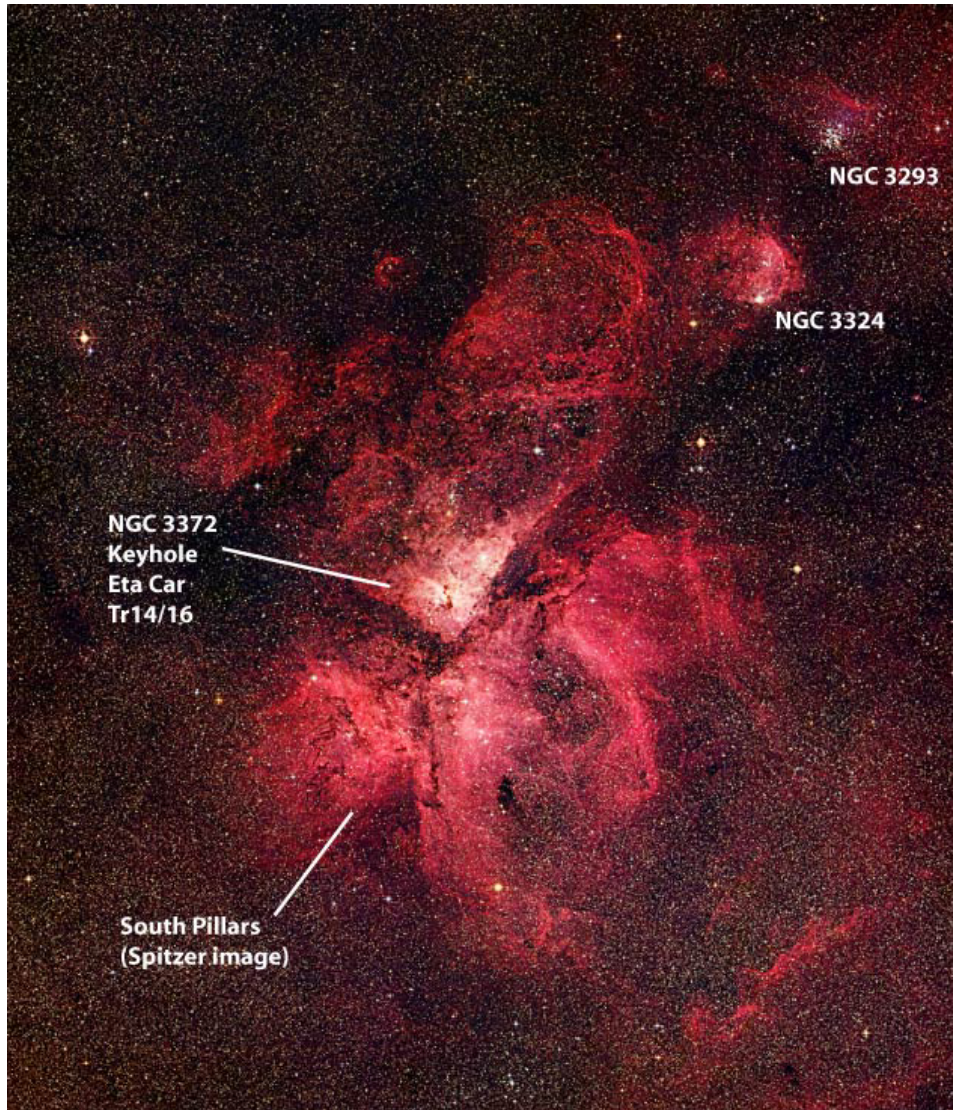


Figure 1. A large field-of-view photograph of the Carina Nebula made from UK Schmidt plates by David Malin. Anglo-Australian Observatory/Royal Obs. Edinburgh.

more extinction. The low extinction toward Carina combined with its proximity and rich nebular content provide a worthwhile trade-off.

For the most massive stars, lifetimes of ~ 3 Myr before they explode as supernovae (SNe) are comparable to the time it takes to clear away their surrounding large-scale distribution of molecular material. Consequently, we already have a situation in Carina where the most massive members like η Car are approaching their imminent demise while new stars are being born from dense molecular gas only 5–20 pc away. In the next 1–2 Myr, there will be several energetic SNe in Carina. These will carve out an even larger cavity in the ISM and form a giant superbubble in the Galactic plane,

and may pollute protoplanetary disks with nuclear-processed ejecta. In the mean time, studying this rich region provides a snapshot of a young proto-superbubble (Smith et al. 2000) energized only by UV radiation and stellar winds, just before the disruptive SN-dominated phase.

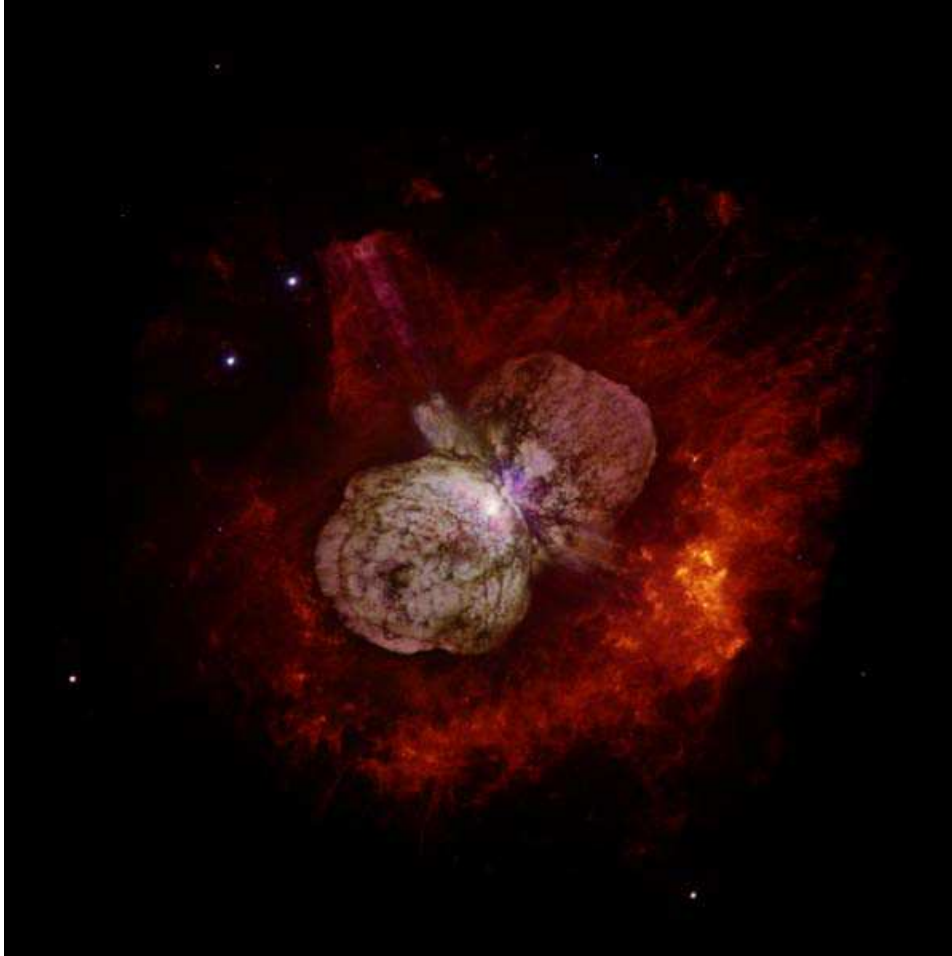


Figure 2. An *HST*/WFPC2 image of η Carinae and its surrounding nebula (N. Smith/NASA).

1.1. The Star: Eta Carinae

From before the time of Herschel up to the present, most observational effort in the Carina Nebula had focussed on the variable star η Carinae (Fig. 2) and its immediate surroundings. The unusual variability of η Car was noted as early as the 17th century by Halley, when it was reputed to vary between 4th and 2nd magnitude. Later, in the early and mid 19th century, it was observed by John Herschel (1847) as it brightened significantly to become the second brightest star in the sky. It then faded from view by the 1870s. Frew (2004) gives a careful and detailed account of the historical light curve (Fig. 3). During that event, the star ejected more than $10 M_{\odot}$ with almost 10^{50}

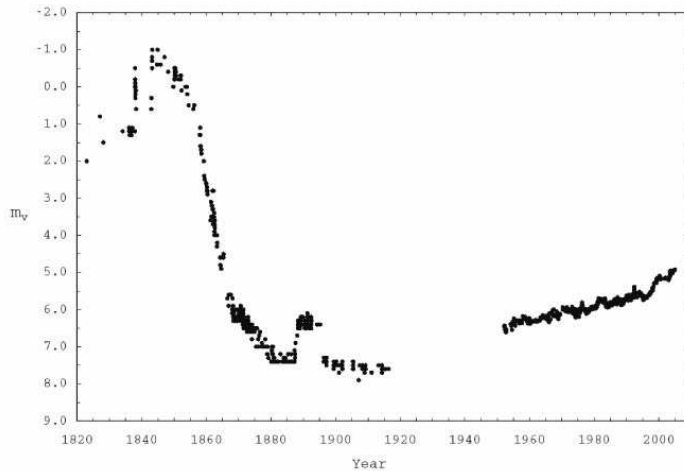


Figure 3. The historical visual light curve of η Carinae (from Frew 2004).

erg of kinetic energy (Smith et al. 2003b), which has since expanded to form the so-called “Homunculus” nebula seen today in *HST* images like the one in Figure 2. After more than 160 years and intensive study at all wavelengths, the underlying cause of this so-called “Great Eruption” is still the most enduring mystery associated with η Car. Additionally, much current work centers around the 5.5-yr periodic variability that is likely the product of η Carinae being an eccentric binary system (e.g., Daminieli et al. 2000).

Our focus here is on star formation in the surrounding giant H II region, so we do not aim to review or summarize the vast and complicated literature concerning η Carinae and its ejecta (see Davidson & Humphreys 1997; although much has been added to our understanding in the subsequent decade making that review outdated in some respects). However, the wild variability of η Car, its extreme nature, and its imminent demise are relevant for nebular structures in the region. From the point of view of understanding star formation in the region, two important facts are most worth remembering:

(1) Although η Carinae is probably the most massive and luminous star known in the Milky Way, *at the current time it contributes essentially nothing to the radiative energy budget of the surrounding region*. This strange twist arises because η Carinae is currently surrounded by a nearly opaque dust shell ejected 160 years ago, which absorbs nearly all of the star’s UV and visual luminosity. That luminosity is then re-radiated in the thermal IR, and it escapes from the nebula, exerting little influence on the surrounding gas in the star-forming complex.

(2) However, before 1843 (for about 3 Myr prior), η Carinae had a tremendous influence on the UV energy budget of the entire region. Its UV luminosity dominated the ionization of the main cavity and it sculpted many of the most prominent elephant trunks in the region. When the giant eruption ended about 150 years ago and η Car faded due to dust obscuration, the UV luminosity of the region dropped by 20% (Smith 2006a) and the remaining O stars that are scattered throughout the region now dominate the ionization. This change, which arises because of η Car’s precarious instability and its evolved state, is unique among Galactic H II regions.

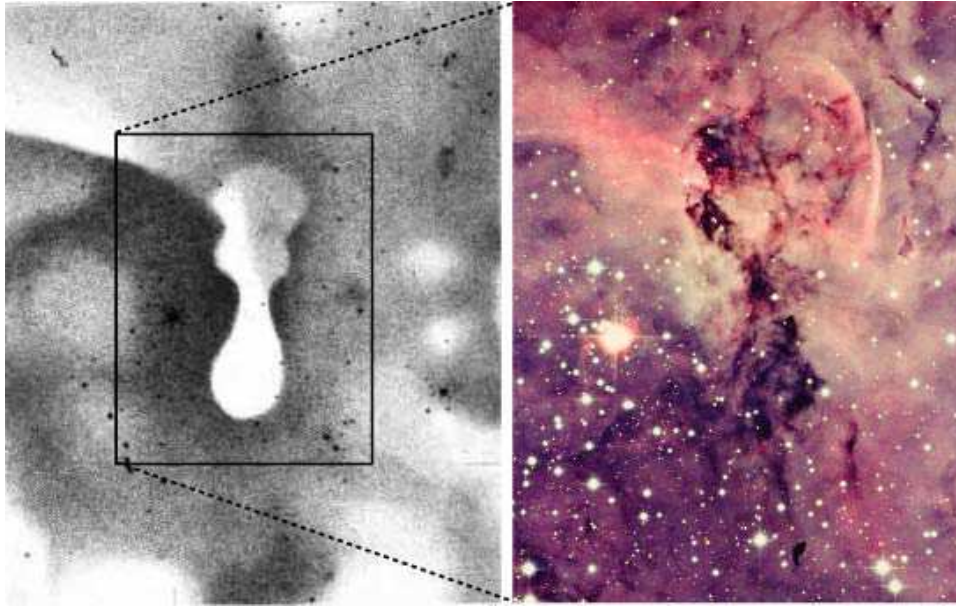


Figure 4. Left: Herschel’s drawing of the Keyhole Nebula, made during η Carinae’s 19th century outburst. Right: A modern color photograph of the Keyhole made by David Malin.

1.2. Historical Perspective: The Keyhole

The famous “Keyhole” nebula at the heart of the greater Carina Nebula also has a rich history, aided by its location immediately adjacent to η Carinae, as well as its extremely high surface brightness. The physical origin of the Keyhole shape is still not understood (although see Smith 2002b).

While the old-fashioned keyhole shape is easily recognized in Herschel’s drawing, more creativity is required to identify this structure in modern photographs (see comparison in Fig. 4). The most dramatic difference is in the lower part of the Keyhole, where much of the diffuse emission is brighter in Herschel’s drawing. This has caused some consternation to observers (e.g., Bok 1932), making some suspect that Herschel may have had an over-active imagination. In fact, it is likely that Herschel’s drawing was largely correct, and that the appearance of the nebula has actually changed with time. Herschel’s drawing in Figure 4 was made around 1840, during the Great Eruption of η Car, before the star was obscured by its dusty nebula. Thus, at that time the Keyhole was illuminated by a much brighter star than is seen today, and the reflection nebulosity around the Keyhole could have differed in appearance. We now know from both historical and modern data that the reflected spectrum of η Car is seen in the Keyhole (Walborn & Liller 1977; Lopez & Meaburn 1986), confirming that it is at the same distance as η Car. Given that the larger Carina Nebula is more than 150 light years across, one might wonder if light echoes from the Great Eruption can still be seen in archival images.

As for the diffuse emission from the larger Carina Nebula, Herschel did have a few choice words to describe it: “It would be manifestly impossible by verbal description to give any just idea of the capricious forms and irregular gradations of light affected by

the different branches and appendages of this nebula.” The rich, complex structure that Herschel was referring to is associated with the many dust pillars and dark globules, the likes of which are not seen in the Orion Nebula. Perhaps this is an early testament to feedback from the extreme stellar population in Carina, providing us with a snapshot of a molecular cloud getting shredded by its progeny.

In the 20th century, observers began to take a broader view of Carina, realizing that it spanned several degrees of the sky. In this review, we are concerned with star formation across the full extent of the Carina Nebula. The nomenclature for this region is interchanged loosely, being referred to variously as NGC 3372, the “Carina Nebula”, the “Great Carina Nebula”, the “Keyhole Nebula”, the “Eta Carinae Nebula”, or (incorrectly) as simply “Eta Carinae”. We reserve “Eta Carinae” for discussions of the massive star itself, the “Homunculus” nebula (Gaviola 1950), plus surrounding ejecta nebulosity within about 1' (e.g. Smith et al. 2005a). We use the name “Keyhole Nebula” to refer to the structures in Figure 4, within about 10' of η Car, while we use the term “Carina Nebula” to refer to the larger giant H II region spanning several square degrees (Fig. 1), of which η Car and the Keyhole are only a small component at the center.

1.3. Pioneering Observations of the Nebulosity

The first modern interference-filter photographs of the region were made by Walborn (1975) and Deharveng & Maucherat (1975). These images showed the complex structures of the Keyhole and the rest of NGC 3372 in ionized gas, and revealed many silhouette structures, such as dust pillars and globules, and the large, dark V-shaped dust lane that bisects the nebula. It was established early on that the V-shaped dark lanes are the result of obscuration by dust intermixed with molecular gas (Dickel 1974; Feinstein et al. 1973; Smith 1987). Far-infrared (far-IR) emission was detected from the dark lanes by Harvey et al. (1979) at 80 μm and Ghosh et al. (1988) at 120–300 μm , implying that the dust was warm, with $T \simeq 30\text{--}40$ K. The first single-dish molecular line studies of Carina by Gardner et al. (1973) and Dickel & Wall (1974) revealed that these dark dust lanes coincided with the bulk of the molecular gas.

Pioneering radio observations of the Carina nebula focused on the central region with angular resolutions (FWHM) that were typically 3' (e.g., Gardner & Morimoto 1968; Shaver & Goss 1970; Gardner et al. 1970; Jones 1973; Dickel 1974; Huchtmeier & Day 1975; Retallack 1983; Tateyama et al. 1991). Gardner et al. (1970) first identified the two bright concentrations known as Car I and Car II (see Fig. 9). Subsequent observations established that these two sources were thermal and represented two separate H II regions. Car I was found to be located toward the north-western part of the inner nebula, and Car II was identified with the central Keyhole Nebula. Retallack (1983) was the first to separate η Car from the bright radio continuum emission of Car II, and to highlight the similar ring-shaped structures of the radio source Car II and the Keyhole Nebula seen at visual wavelengths.

Detections of non-thermal emission toward the nebula were reported by Jones (1973) and Tateyama et al. (1991). However, no subsequent work has found convincing evidence to confirm these non-thermal sources. The non-thermal source G287.7–1.3 first reported by Shaver & Goss (1970) has since been shown to be extragalactic (Caswell & Haynes 1975). The magnetar studied by Gaensler et al. (2005) is located at a larger distance and well outside the Carina Nebula 1° to the east.

It is amusing to note that the first large-scale CO study of the Carina Nebula at 115 GHz used the *optical* ESO 3.6-m telescope at La Silla in 1978 (de Graauw et al. 1981).

These data were soon followed by the CO survey undertaken by Whiteoak & Otrupcek (1984) using the 4-m radio telescope in Sydney. The resulting maps with a $\sim 2'$ (FWHM) beam offered the most detailed view of the Carina molecular cloud for more than a decade, and showed that the bulk of the molecular material was concentrated into a northern and a southern cloud. The total extent of the molecular cloud was revealed later in the Columbia CO survey of the Galactic plane (Grabelsky et al. 1988). The survey showed that the Carina molecular cloud is part of a GMC complex that is situated on the near side of the Carina arm and extends over 150 pc between $l=284.7$ and 289, with a total estimated mass of $6.7 \times 10^5 M_{\odot}$.

Results from the first studies of the velocity field within the Carina Nebula showed complex structure that is still not understood. Interpretations of the large-scale dynamics measured across the nebula involved merging spiral arms (Tateyama et al. 1991), rotating neutral clouds (Meaburn et al. 1984) or old H II regions (Cersosimo et al. 1984). On a smaller scale, the complicated dynamics measured in the vicinity of Car II alluded to the tremendous influence of the stellar wind from η Car. Motions of ionized gas were studied via radio hydrogen recombination lines (e.g. Gardner et al. 1970; Huchtmeier & Day 1975; Cersosimo et al. 1984) and optical-line emission profiles (e.g. Deharveng & Maucherat 1975). All studies detected double-peaked profiles in the vicinity of Car II. Deharveng & Maucherat (1975) proposed that the ionized gas lies in an expanding shell whose center of expansion is η Car.

Additional evidence for peculiar, high-speed gas motions in the vicinity of η Car has been seen in resonance-line absorption profiles (Walborn & Hesser 1975). These unusual multi-component profiles have received continued study in the optical and UV (Walborn 1982; Walborn & Hesser 1982; Laurent et al. 1982; Garcia & Walborn 2000; Walborn et al. 2002a, 2007), but are still not understood. Velocity components range over 500 km s^{-1} and have sometimes been interpreted as evidence for a supernova remnant along the line of sight, although proof of this hypothesis remains elusive. Elliot (1979) interpreted broad emission components as evidence for a supernova remnant in the Keyhole, but these were actually broad lines in the wind spectrum of η Car itself that were reflected by dust in the Keyhole (see Walborn & Liller 1977; Lopez & Meaburn 1986).

Nevertheless, there are a few observational clues that hint at a possible young supernova remnant (SNR) inside Carina. In addition to the complex blueshifted absorption lines already noted, IR spectroscopy with ISO revealed an unusual and strong broad $22 \mu\text{m}$ emission feature, attributed to silicates by Chan & Onaka (2000), who note that the only other source where a similar emission feature is seen is the young supernova remnant Cas A. Carina also displays spatially extended diffuse soft X-ray emission across much of its central $\sim 1^{\circ}$ region. The diffuse X-ray emission was first detected in *Einstein* data by Seward et al. (1979), although Seward & Chlebowski (1982) concluded that the diffuse emission could be accounted for simply by mechanical energy input from stellar winds. We discuss this further in Sect. 8.2.

1.4. Prevailing View of Star Formation in Carina

Early far-IR and molecular surveys described above found no luminous, embedded sites of active star formation in the bright central region of the nebula. Additionally, no bright maser sources were identified in the region (e.g., Caswell 1998). Hence, the prevailing view until the mid-1990s was that Carina was an evolved H II region devoid of active star formation.

This view has changed dramatically in recent years, due in part to larger spatial coverage and higher-quality data at IR and radio wavelengths. In just the past decade, the Carina Nebula has been recognized as a hotbed of active, ongoing star formation where the star formation is occurring primarily at the periphery of the nebula (Smith et al. 2000; Megeath et al. 1996). It provides a laboratory to study several star formation phenomena in great detail, all of which have recently been identified here: (1) evaporating protoplanetary disks (the so-called “proplyds”), small cometary clouds, or globules (Smith et al. 2003a, 2004b; Smith 2002b; Brooks et al. 2000, 2005; Cox & Bronfman 1995), (2) the erosion of large dust pillars and the triggering of a second generation of star formation within them (Smith et al. 2000, 2005b; Rathborne et al. 2004; Megeath et al. 1996), (3) irradiated Herbig-Haro (HH) jets that signify active accretion (Smith et al. 2004a), (4) photodissociation regions (PDRs) on the surfaces of molecular clouds across the region (Brooks et al. 2003, 2005, 1998; Rathborne et al. 2002; Smith et al. 2000; Smith & Brooks 2007; Mizutani et al. 2004), and on the largest scales, (5) the early stages of a fledgeling superbubble (Smith et al. 2000; Smith & Brooks 2007).

Most of the current star-formation activity seems to be occurring near the edges of the nebula, although this is not strictly true as some of the most recent data show. In general, the central clusters Tr 14 and Tr 16 tend to be devoid of star formation. DeGioia-Eastwood et al. (2001) and Tapia et al. (2003) noted the presence of young stars with IR excess in these clusters, but these were consistent with age spreads of several million years among the low/intermediate-mass stellar population. Similarly, Sanchawala et al. (2007) noted that ~ 300 X-ray sources in these clusters have properties consistent with low/intermediate-mass pre-MS stars. In any case, the most active sites of ongoing star formation are not the central clusters, but the outlying areas of the nebula.

Because of its proximity, large size on the sky, and its extreme nature, the level of detail we can observe in the Carina Nebula makes it appear bewilderingly complex, and it is just beginning to reveal its secrets to us. The following sections focus on some of the recent work that has shed new light on Carina as an active star forming region.

2. Neighborhood, Distance, and Reddening

The Carina Nebula resides in one of the richest regions of the Milky Way, from the point of view of massive star formation. Figure 5 shows the part of the Galactic plane in Carina surrounding the Carina Nebula. This direction looks nearly down the tangent point of the Sagittarius-Carina spiral arm, and several massive star-forming regions are seen. To the left of Carina (in the direction of the Galactic center) are the rich massive cluster NGC 3603 and the spectacular H II region NGC 3576. To the right of Carina is RCW 49, made famous recently by Spitzer images (Whitney et al. 2004) with its extremely massive cluster Westerlund 2. Carina is several times larger, brighter, and closer than these other regions, many of which are at the far kinematic distance of 6–8 kpc and highly reddened.

Unlike most massive star forming regions, the distance to the Carina Nebula is known accurately. A distance of 2.3 kpc (accurate to $\pm 2\%$) comes primarily from the expansion parallax of the Homunculus nebula around η Carinae (Smith 2006b, 2002a; Allen & Hillier 1993), combined with the fact that η Car itself is known to be within the Carina Nebula because its reflected light is seen across the Keyhole Nebula (Walborn & Liller 1977; Lopez & Meaburn 1986) and because the Homunculus occults light from

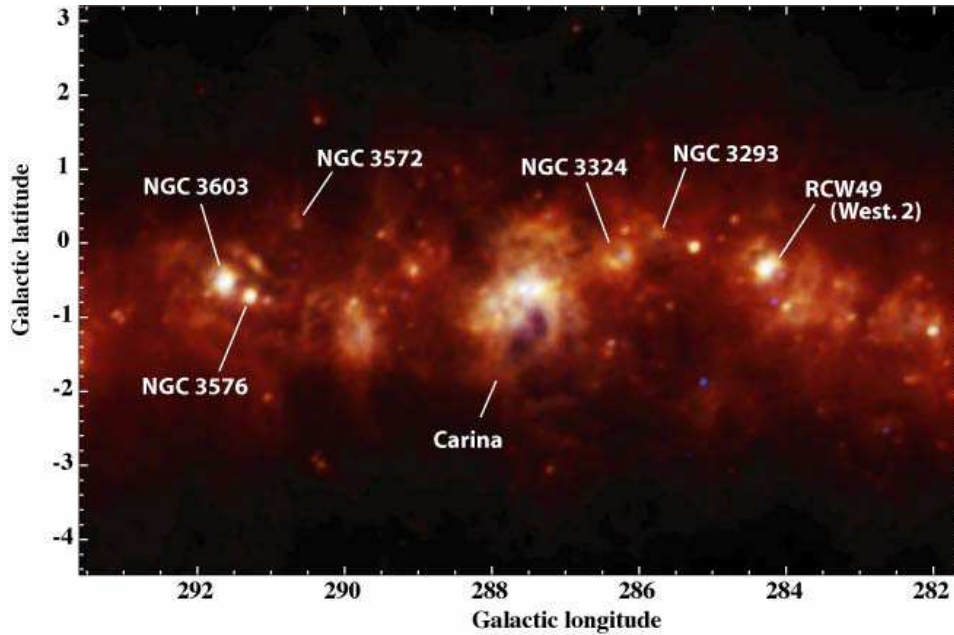


Figure 5. The Milky Way in Carina observed by IRAS at $25\ \mu\text{m}$ (blue), $60\ \mu\text{m}$ (green), and $100\ \mu\text{m}$ (red). Several other well-known regions are labeled.

the back side of the nebula but not the front (Allen 1979). In general, this distance agrees with favored values derived for the star clusters in Carina as well (Walborn 1995; Thé & Vleeming 1971), although a range of values up to several kpc has been reported. Caution is always wise, however, as the sightline toward Carina looks down a tangent of a spiral arm as noted above. To be more precise, this is the distance to η Car, the Keyhole, and Tr 16. One normally assumes that the other clusters described below (Tr 14, Cr 228, etc.) are not at vastly different distances since they appear to be involved in the same larger nebulosity and share similar kinematics. This has been the topic of some debate, however.

Our sightline to the Carina Nebula also suffers little extinction and reddening compared to most massive star forming regions, affording us the opportunity for detailed visual-wavelength studies of the stars and fainter nebulosity. Values of only $E(B - V) = 0.5$ are favored for the visible star clusters (Walborn 1995; Feinstein et al. 1973, 1980), although a casual look at an optical image reveals that extinction is highly position-dependent in the nebula. The reddening law toward Carina is anomalous, with $R \sim 4-5$ instead of 3.1 (Herbst 1976; Forte 1978; Thé et al. 1980; Smith 1987; Smith 2002b). Thé et al. (1980) noted that the reddening law varies along different lines of sight in the same nebula, which continues to dominate the uncertainty in photometric and spectroscopic distance determinations.

3. Stellar Content: Eta Carinae and its Siblings

The Carina Nebula is probably best known as the dwelling of our Galaxy's most luminous, massive, and unstable star – η Carinae. While on the main sequence, this one

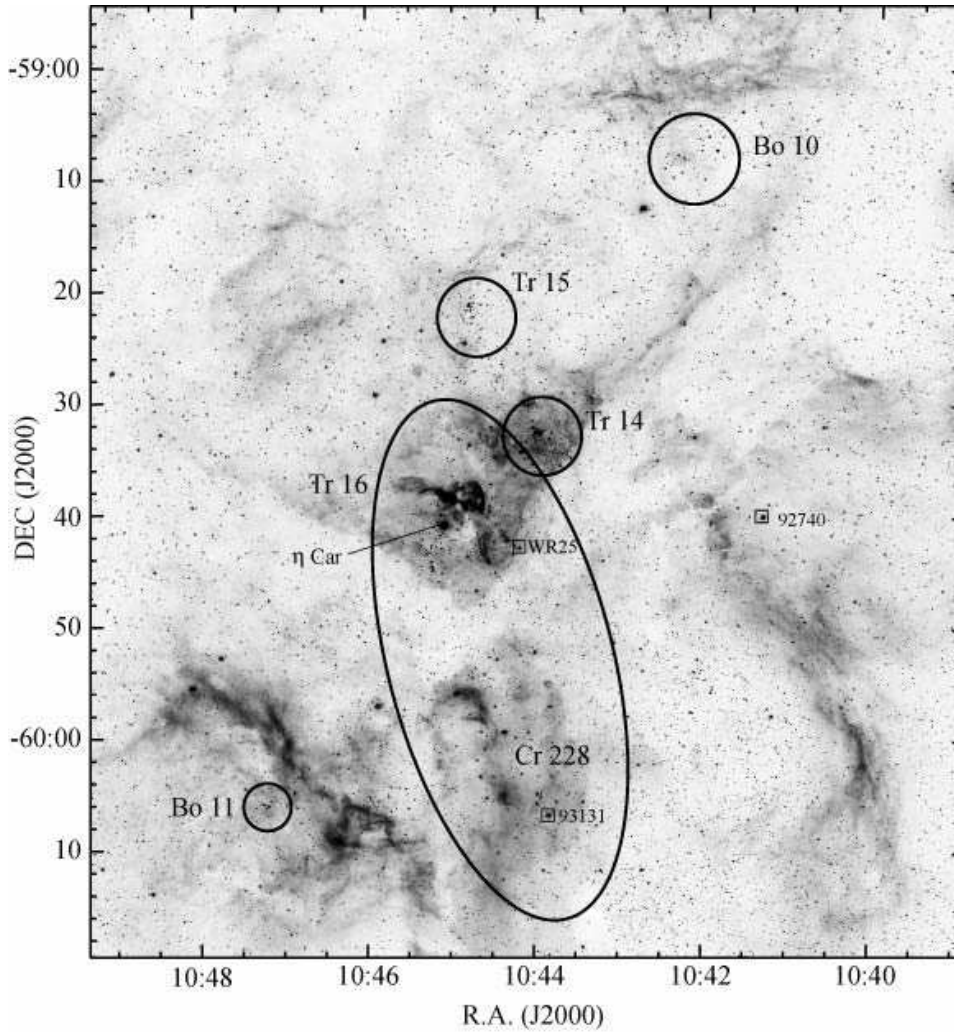


Figure 6. A [S II] image of the Carina Nebula identifying the approximate locations of the star clusters in Table 1: Trumpler 14, 15, and 16, and Bochum 10 and 11. Note that Collinder 228 is generally considered to be part of Tr 16, but these appear as two clusters on the sky because they are divided by an obscuring dust lane. The location of η Carinae is given, and the three WNH stars are identified with small squares: WR25 (HD 93162), HD 93131, and HD 92740. The CTIO Schmidt image is from Smith et al. (2004a).

star dominated the evolution of the surrounding H II region. However, η Car often outshines its several spectacular neighbors that also occupy the interior of the Carina Nebula, distributed in several sub-clusters (Fig. 6). In addition to η Car itself, Carina boasts an O2 supergiant (HD 93129A; Walborn et al. 2002b), three WNH stars (late-type WN stars with hydrogen; see Smith & Conti 2008; Crowther et al. 1995) that are likely near the end of core-H burning and are probable descendants of O2 supergiants, several O3 stars, and more than 60 additional O stars (see Smith 2006a). Carina also hosts a B1.5 supergiant with a ring nebula (SBW1) that is nearly identical to those of

Sher 25 and the progenitor of SN1987A in NGC 3603 and 30 Dor, respectively (Smith, Bally, & Walawender 2007). This is only the confirmed, optically-visible O star population; for example, Sanchawala et al. (2007) have recently identified 16 additional OB candidates that suffer high extinction and are only seen in the IR. With all these O-type stars, the Lyman continuum output and total stellar content of Carina are about the same as NGC 3603, and are 25-30% of the Arches cluster and R136 in 30 Dor (see Smith 2006a). This fact is often overlooked in studies of massive clusters because the O stars in Carina constitute a looser proto-OB association (Fig. 6), rather than a single dense cluster.

Because of its remarkable stellar content and observability, Carina has often been in the forefront of understanding very massive stars. For example, Carina is the first place where the (then) earliest spectral type O3 stars were recognized (Walborn 1973), and is the first place where an O2 Iaf* supergiant was classified (Walborn et al. 2002a). There is much more to tell, but our goal here is to discuss star formation in Carina, so we do not give an adequate summary of work on the remarkable stellar content in this region; for reviews, see Walborn (1995; 2002), Feinstein (1995), Tapia (1995), or Massey & Johnson (1993).

Relatively little work has been done on the low-mass pre-main-sequence stellar population in Carina, even in the Tr 14 and 16 clusters. Schwartz et al. (1990) presented a survey for H α emission-line stars, but a more complete and detailed census of the young pre-main-sequence stars is still waiting to be done. A recent study of deep *JHK* photometry of Tr 14 (Ascenso et al. 2007) has made significant progress in this direction (see Fig. 7).

Since our main focus here is on current (i.e. ongoing) star formation in Carina, we do not review the full literature on photometry and spectroscopy of the stars in the component clusters of the Carina Nebula (Fig. 6). Some references for each cluster are: Tr 14 (Thé et al. 1980; Tapia et al. 1988; Morrell et al. 1988; Massey & Johnson 1993; Vazquez et al. 1996; Garcia et al. 1998; Ascenso et al. 2007), Tr 15 (Thé et al. 1980; Morrell et al. 1988; Carraro 2002), Tr 16 (Feinstein 1982; Levato et al. 1991; Massey & Johnson 1993; Kaltcheva & Georgiev 1993), Cr 228 (Carraro & Patat 2001), Cr 232 (Carraro et al. 2004), Bo 10/11 (Feinstein 1982; Fitzgerald & Mehta 1987). There are also some general studies of the stellar content of multiple clusters (Sher 1965; Moffat & Vogt 1975; Shobbrook & Lynga 1994; Tapia et al. 2004) and the larger Car OB1 (Humphreys 1978). Two adjacent star clusters that are not actually part of the Carina Nebula (see Figure 1) are NGC 3293 (Turner et al. 1980; Feinstein & Marraco 1980; Shobbrook 1980) and NGC 3324 (Carraro et al. 2001).

We limit the remaining discussion here to the collective energy input and feedback caused by these stars (summarized from Smith 2006a). These stars are distributed among 5 main visually-identified clusters listed in Table 1 and shown in Figure 6, although Trumpler 16 at the center of the H II region dominates all others in terms of stellar mass and energy input. Tr 14 is a close second; Tr 15 and Bochum 10 and 11 are unimportant globally, but they influence their local environments. With these stars residing in several loose clusters rather than one supercluster, Carina represents the birth of an unbound OB association. There may be a mild age-spread in the various clusters (see Smith 2006a; DeGioia-Eastwood et al. 2001). Tr 16 is thought to be ~ 3 Myr old, since η Car and the three WNH stars have reached the end of their main-sequence evolution. Based on the magnitudes of O stars and its compact structure, Tr 14 is somewhat younger, perhaps 1–2 Myr. The northern clusters Tr 15 and Bo 10 are probably older,



Figure 7. A *JHK* image of the Tr 14 cluster (from Ascenso et al. 2007).

at several Myr. Bo 11 is very young at $\lesssim 1$ Myr, which is interesting since it is located amid the South Pillars (see below). Nearby, the semi-embedded “Treasure Chest” cluster around CPD-59°2661 is probably only ~ 0.1 Myr old (Smith et al. 2005b). Ages of these clusters, especially Tr 14 and 16, are relevant to the properties of the ionized and molecular gas in the region.

Table 1 lists the total number of O stars, bolometric luminosity, ionizing flux, mass loss, and mechanical luminosity for each cluster, as well as the cumulative total of all clusters (for more details see Smith 2006a and references therein). For the cumulative effects, two distinct cases are important: The first case (**MS**) corresponds to the history of Carina up until recent times, when η Car was on the main sequence, so that the massive binary was not surrounded by a dust shell and did not have a dense LBV wind choking off its Lyman continuum flux, and when the WNH stars in Tr 16 were presumably O2 stars as well. For this first case, there were a total of 70 O-type stars in Carina, producing at least $Q_H \simeq 1.2 \times 10^{51} \text{ s}^{-1}$. This would be the appropriate number to adopt when considering the history and formation of the nebula, the lifetimes of evaporating

Table 1. Total Stellar Energy Input (from Smith 2006a)

Cluster	Number of O stars	log L (L_{\odot})	log Q_H (s^{-1})	\dot{M} ($10^{-6} M_{\odot} \text{ yr}^{-1}$)	L_{SW} (L_{\odot})
Tr 16 (MS)	47	7.215	50.91	91	45400
Tr 16 (now)	42	7.240	50.77	1083	67000
Tr 14	10	6.61	50.34	18.7	13500
Tr 15	6	6.18	49.56	5.9	1410
Bo 10	1	6.00	49.42	18.3	7120
Bo 11	5	6.00	49.64	5.2	2900
(CPD-59°2661)	1	4.68	47.88	0.15	33
TOTAL (MS)	70	7.38	51.06	139	70300
TOTAL (now)	65	7.40	50.96	1131	91900

proplyds, globules, and dust pillars, triggered star formation by radiative driven implosion, and the growth of the cavity that will blow out of the Galactic plane as a bipolar superbubble (Smith et al. 2000). The second case (**now**) corresponds to the presently-observed state of the Carina Nebula, when η Car and its companion are surrounded by an obscuring dust shell, blocking all their contribution to the total ionizing flux. With η Car and its companion blocked by the Homunculus, the effective number of O stars is reduced to 65 (the three WNH stars have also evolved off the main sequence, although they still contribute very strong Lyman continuum radiation). For this case, the cumulative ionization source is $Q_H=9 \times 10^{50} \text{ s}^{-1}$. This is the number to adopt for the *current* UV flux incident upon evaporating proplyds, globules, and irradiated jets, as well as the current energy budget of the region (Smith & Brooks 2007).

For most of its lifetime, gas and dust in Carina has been exposed to an ionizing luminosity about 150 times stronger than that of the Orion Nebula. This changed 160 years ago when η Car ejected a thick dust shell that cut off essentially all of its UV output, and the total Q_H of the Carina Nebula dropped by about 20% due to the loss of ionization from the region's most luminous member, as noted earlier in Sect. 1.1. Some dark globules seen only in silhouette today were exposed to the harsh ionizing radiation from η Carinae in the past (Smith et al. 2003a). This variable UV output of the central engine makes Carina a unique laboratory for studying feedback effects.

4. Global Properties of the Nebulosity

Elsewhere (Smith & Brooks 2007), we have recently summarized the global properties of the nebula and analyzed its energy budget. The main properties to note from that study are the following:

- The total IR luminosity of $1.2 \times 10^7 L_{\odot}$ is about half of the known stellar luminosity of O stars, so about half the UV radiation from these stars escapes the giant H II region.
- The number of ionizing photons inferred from the total radio continuum and $H\alpha$ both underestimate the known ionizing photon flux from the O stars (Smith 2006a). Radio continuum seems to trace $\sim 75\%$ of the ionizing flux, while $H\alpha$ is far worse because of extinction, yielding a value only half that of the radio continuum. This

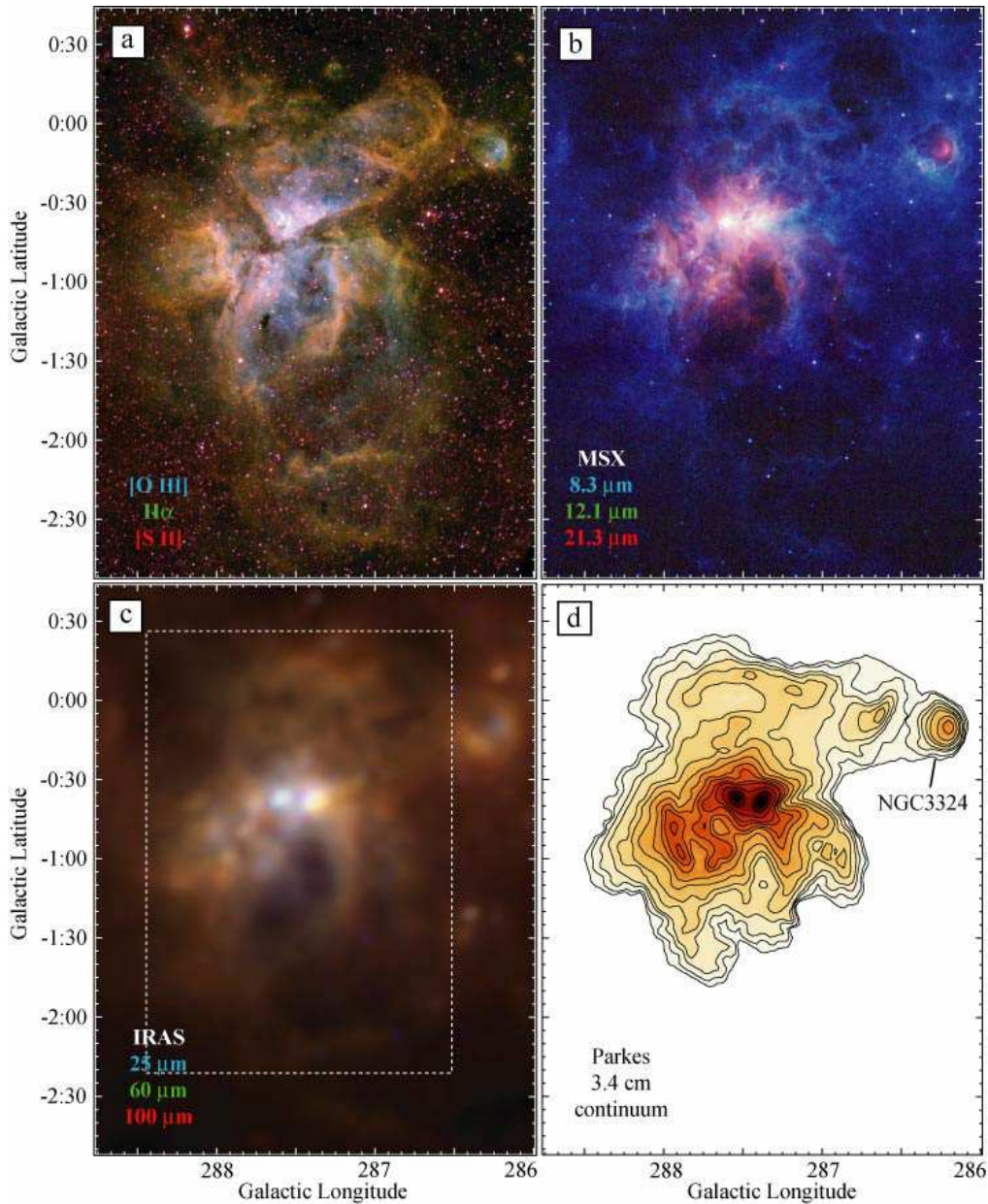


Figure 8. A large-scale multiwavelength view of the entire Carina Nebula from Smith & Brooks (2007). (a) Composite color visual image with blue = $[\text{O III}] \lambda 5007$, green = $\text{H}\alpha$, and red = $[\text{S II}] \lambda\lambda 6717, 6731$ (from Smith et al. 2000). (b) Color image from MSX data, with blue = Band A, green = Band C, and red = Band E. (c) Color image from IRAS data, with blue = $25 \mu\text{m}$, green = $60 \mu\text{m}$, and red = $100 \mu\text{m}$. (d) False color image of the 3.4 cm radio continuum measured by the Parkes telescope (see Huchtmeier & Day 1975). The dashed rectangle in Panel (c) is the region over which Smith & Brooks (2007) integrated the total flux at all wavelengths. The axes are labeled in degrees of Galactic coordinates. On the largest scales, the nebula appears to be bipolar, with an axis perpendicular to the Galactic plane.

might be useful for interpreting observations of unresolved extragalactic H II regions (see Smith & Brooks 2007 for additional discussion).

- Emission from warm dust that dominates the SED at $\sim 20 \mu\text{m}$ has the same spatial distribution as the radio continuum (see Fig. 4c of Smith & Brooks 2007). This warm $\sim 80 \text{ K}$ dust is therefore intermixed with ionized gas in the interior of the H II region, and would not be a useful tracer of emission from star forming cores in more distant unresolved regions.

- Similarly, cooler dust at 30–40 K that dominates the far-IR emission at 60–100 μm is spatially correlated with diffuse PAH emission (see Fig. 4d of Smith & Brooks 2007). We therefore suggested that the far-IR emission traces primarily atomic gas in PDRs at the surfaces of molecular clouds, while dust within the molecular clouds will be even cooler, emitting primarily at submm wavelengths where observations are still incomplete.

- The 30–40 K dust indicates a total emitting dust mass of $\sim 10^4 M_{\odot}$. With a normal gas:dust mass ratio of 100, the $10^6 M_{\odot}$ of atomic gas mass located in neutral PDRs significantly outweighs the molecular gas mass in the nebula, which is a few times $10^5 M_{\odot}$. This is a vital clue to the current state of star formation in an evolved H II region like Carina, because it means that the majority of the nebular mass that is present is atomic rather than molecular, and therefore represents a huge mass reservoir that is not being tapped for current star formation. Smith & Brooks (2007) give a fuller discussion of this.

Analogous to the overall structure of 30 Doradus in the LMC, the Carina Nebula gives us a snapshot of a giant molecular cloud being blasted apart by UV radiation and stellar winds from the massive stars it has given birth to. Deep images of nebular emission at visual wavelengths (Fig. 8a; Smith et al. 2000) show limb-brightened filaments and bubbles spanning more than 3° or 120 pc, with many dark obscuring dust features. IR emission is also seen across the same large region, mainly due to PAH emission from PDRs at the surfaces of illuminated molecular clouds seen in the 8 μm MSX image in Figure 8b, and thermal emission from warm dust at longer wavelengths in IRAS images (Fig. 8c). The MSX image in Figure 8b, in particular, gives the impression that the Carina Nebula consists mainly of a large bipolar cavity that is being carved with an axis perpendicular to the Galactic plane (Smith et al. 2000). A series of large shells seem to be breaking out of the Galactic plane toward the lower right in this image (Smith et al. 2000); this is the direction we might expect these old shells to follow if they are being distorted by Galactic shear.

The pair of images in Figure 9 demonstrate the relationship between the molecular cloud, the ionized gas and the IR dust emission across the brightest part of the nebula. The left panel in Figure 9 shows a zoomed-in view of the 8 μm MSX emission described earlier. The image is dominated by the spectacular southern dust pillars, some with bright compact emission sources at their tips. The two radio continuum sources Car I and Car II can be identified in the right panel of Figure 9. This 0.843 GHz (36 cm) radio continuum image (Whiteoak 1994) has been taken from the Molonglo Galactic Plane Survey (MGPS) made with the Molonglo Observatory Synthesis Telescope (MOST). The contours overlaid on both the MSX and MOST images represent the NANTEN ^{12}CO data at 115 GHz with a $2.7'$ beam (Yonekura et al. 2005). The data have been integrated over the velocity of range -25 to -15 km s^{-1} (LSR), where the bulk of the molecular gas is found (Lee et al. 2000). The molecular gas is concentrated into three components that have been labeled “Northern Cloud”, “Southern Cloud” and

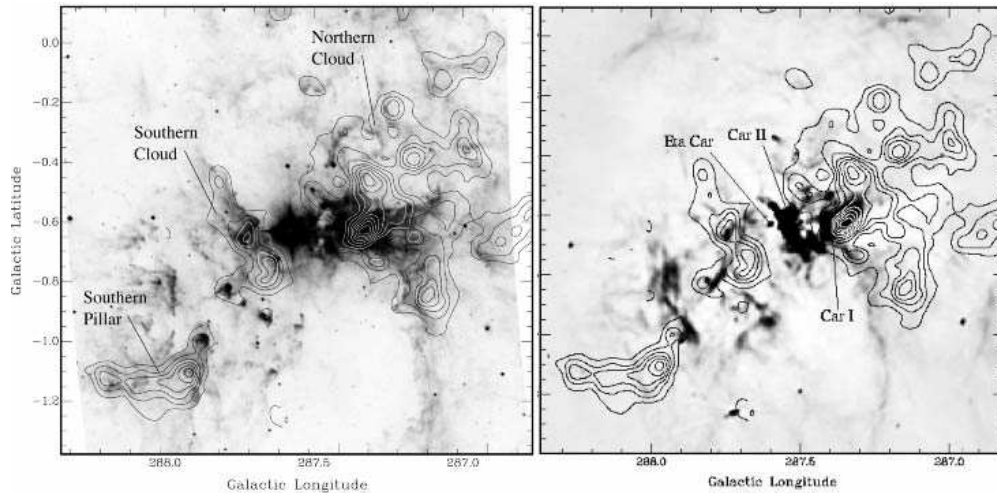


Figure 9. Molecular gas distribution in the Carina Nebula, with contours from the NANTEN $^{12}\text{CO}(1-0)$ survey of Yonekura et al. (2005). These contours are superposed on images at $8\ \mu\text{m}$ from MSX (left; Smith et al. 2000) and in the $0.843\ \text{GHz}$ continuum from MOST (right; Whiteoak 1994).

“Southern Dust Pillar”. The first two components are the same northern and southern cloud components identified in the previous CO survey work of de Graauw et al. (1981), Whiteoak & Otrupcek (1984) and more recently Brooks et al. (1998). The third molecular component traces the giant pillar first identified by Smith et al. (2000).

Figure 9 illustrates the close correspondence between the molecular gas and the MSX $8\ \mu\text{m}$ emission that exists throughout the nebula, and in particular at the edges of the molecular clouds facing η Car. This supports the finding by Zhang et al. (2001) for wide-spread PDR emission throughout Carina. Using the Antarctic Submillimeter Telescope and Remote Observatory (AST/RO), Zhang et al. (2001) obtained fully sampled maps of the Carina GMC complex in the CO(4–3) and [C I] transitions at 460 GHz and 492 GHz, respectively, with a $\sim 3'$ (FWHM) beam. Both of these transitions probe warm ($T \simeq 50\ \text{K}$) and dense ($n_e > 10^3\ \text{cm}^{-3}$) gas associated with PDRs. Using the CO(1–0) and CO(4–3) data they derived average excitation temperatures of 30–50 K. Further confirmation of the widespread PDR emission in Carina comes from the results of $3.29\ \mu\text{m}$ PAH observations using the SPIREX/Abu telescope at the South Pole (Rathborne et al. 2002). A well established tracer of PDR emission, the $3.29\ \mu\text{m}$ PAH emission correlates very well with MSX $8\ \mu\text{m}$ PAH emission. As noted earlier, Smith & Brooks (2007) showed that the PAH emission is, in turn, well correlated with the 30–40 K dust emission that dominates the far-IR SED, and the neutral gas mass of 10^6 traced by that dust represents the dominant phase of nebular material in Carina.

From the point of view of star formation occurring in molecular clouds, this global view of Carina suggests three main areas of interest, sampling three different phases in the development of a GMC: 1) The Keyhole region and its small molecular globules represent the last shredded bits of a GMC core that has already formed a massive cluster; 2) the northern cloud near the Tr 14 cluster represents a relatively pristine GMC that does not yet seem to have very active star formation, but is clearly being irradiated by a massive cluster; and 3) the southern cloud and south pillars represent a region

that is currently being eroded and shaped by radiation and winds from a young massive cluster, giving rise to numerous dust pillars with a second generation of stars forming within them. These three regions will be discussed in the following sections.

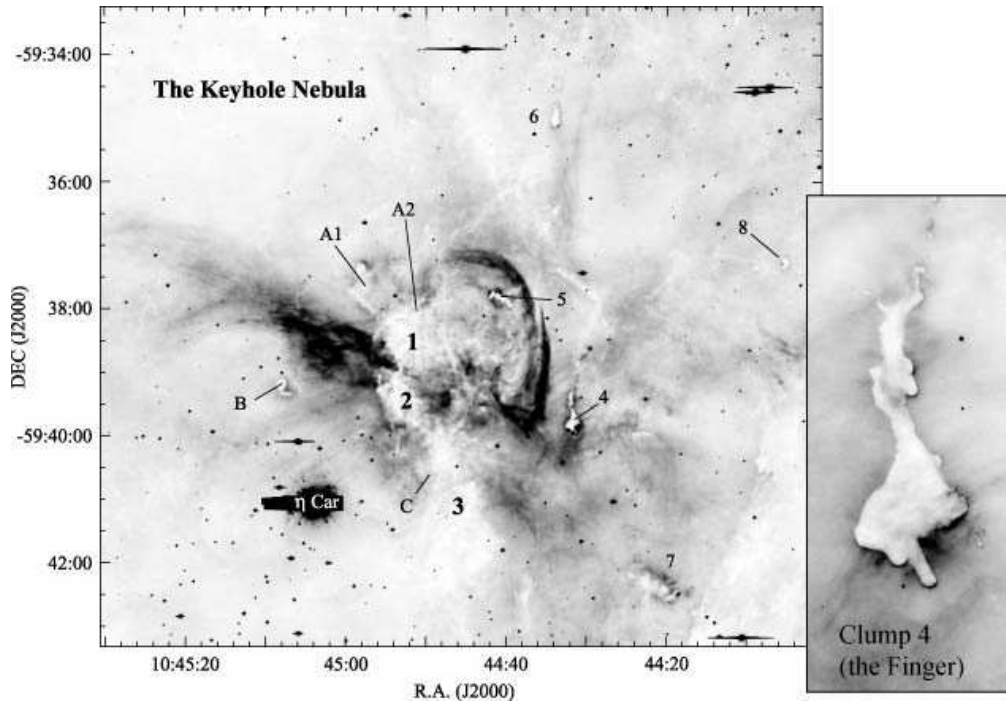


Figure 10. An $H\alpha$ image of the Keyhole nebula and its molecular globules, obtained with the MOSAIC2 camera on the CTIO 4m telescope (see Smith et al. 2003a); see Table 2 for details. The detail of the “Finger” (clump 4) is an $H\alpha$ image obtained with HST/WFPC2 (Smith et al. 2004b).

5. Main Regions of Interest I: The Keyhole and Tr 16

The Keyhole Nebula, located in the center of the larger Carina Nebula about $3'$ from η Carinae within the Tr 16 cluster, is one of the brightest emission-line nebulae in the sky (Fig. 10). In fact, the ionized gas emission is so bright that the strong 1.2 mm continuum emission is dominated by free-free, not cool dust (Brooks et al. 2005) – a property that is rare among star-forming regions. It has a strange arc-shaped structure superposed with many dark obscuring clumps that give it the appearance of an old-fashioned keyhole shape. The velocity field in $H110\alpha$ emission does not match the simple picture of an expanding bubble centered on η Car (Brooks et al. 2001), as had been suggested from earlier work (see Sect. 1.2). Despite its prominence, the physical origin of this structure remains a mystery, although a direct association with η Car has been proposed (Smith 2002b). Many small molecular globules scattered around the Keyhole (Cox & Bronfman 1995; Brooks et al. 2000) suggest that the Keyhole and its associated globules may be the last vestiges of the original molecular cloud core that spawned Tr 16.

Table 2. Molecular globules around the Keyhole

Clump	α_{2000}	δ_{2000}	M/M_{\odot}	Comment
A1	10 44 57.5	-59 37 40	14-19	Kangaroo Nebula
A2	10 44 51.5	-59 38 00	16	...
B	10 45 07.9	-59 39 13	3-5	...
C	10 44 50.4	-59 40 35	6-8	...
1	10 44 52.8	-59 38 27	17	Dark cloud
2	10 44 53.4	-59 39 25	11	Dark cloud
3	10 44 46.0	-59 41 30	4	Dark cloud
4	10 44 31.4	-59 38 48	5-6	The Finger
5	10 44 40.4	-59 37 51	1	...
6	10 44 33.8	-59 35 00	5-10	...
7	10 44 20.5	-59 42 26	3-12	...
8	10 44 05.1	-59 37 16	9-91	...

These small Bok globules are analogous to Thackeray’s globules in IC 2944 (Thackeray 1950a; Reipurth et al. 2003). They have typical sizes of 0.1–1 pc and masses of a few to 10 M_{\odot} , as listed in Table 2 (see Cox & Bronfman 1995; Brooks et al. 2000, 2005; Smith et al. 2004b; Smith 2002b). Whether or not they are sites of ongoing or potential future star formation remains an open question. No embedded IR sources inside these Keyhole globules have been reported yet, but a detailed analysis of one source (the so-called “Finger”; see Fig. 10) indicates that it is currently experiencing external overpressure and may therefore be encountering radiative-driven implosion (Smith et al. 2004b). The globules are massive enough and in a harsh-enough environment that they are good candidates for sites of future triggered star formation.

The enigma of the dark keyhole structure dates back to 1830s and the first detailed drawings of the Keyhole by Herschel (see Sect. 1.1 and Fig. 4). Cox & Bronfman (1995) detected molecular emission from three dark clumps labeled clumps 1, 2 and 3 in Figure 10, with mass estimates from $^{12}\text{CO}(2-1)$ observations of 17, 11, and 4 M_{\odot} , respectively. Unlike the other molecular condensations, clumps 1, 2, and 3 lack bright $\text{H}\alpha$ emission rims and PDR emission (Brooks et al. 2000; Rathborne et al. 2002; Smith 2002b; Walborn 1975). Nor were they detected in the 1.2-mm continuum (Brooks et al. 2005), suggesting lower temperatures than the other clumps. For a clump of 10 M_{\odot} and $T_d = 10$ K, we expect a flux density at 1.2 mm of 0.033 Jy, equivalent to the 2σ observed detection limit. The absence of 1.2-mm emission requires that the dark Keyhole structure is comprised of cool ($T_d < 15$ K) foreground molecular clumps at the outskirts of the H II region (Brooks et al. 2000). The three dark Keyhole clumps may provide a snapshot of an earlier phase that the bright-rimmed molecular globules in the nebula have already passed through – before they were pressure confined and externally photoevaporated. This is supported by the fact that the dark Keyhole clumps are bigger, more massive, darker, and more diffuse than the others. The bright-rimmed globules are being photoevaporated by radiation from Tr 16, while the dark clumps are somehow shielded even though they are projected in almost the same place.

By contrast, Carina also contains many smaller condensations and cometary clouds – the so-called proplyd candidates (Smith et al. 2003a). These much smaller objects are probably in a *more* advanced stage of photoevaporation, with only their dense circumstellar envelopes remaining. It will be an interesting goal for future studies to determine if these objects harbor young stars. The proplyd candidates are scattered throughout the H II region, and some are bright objects while others are seen only in silhouette.

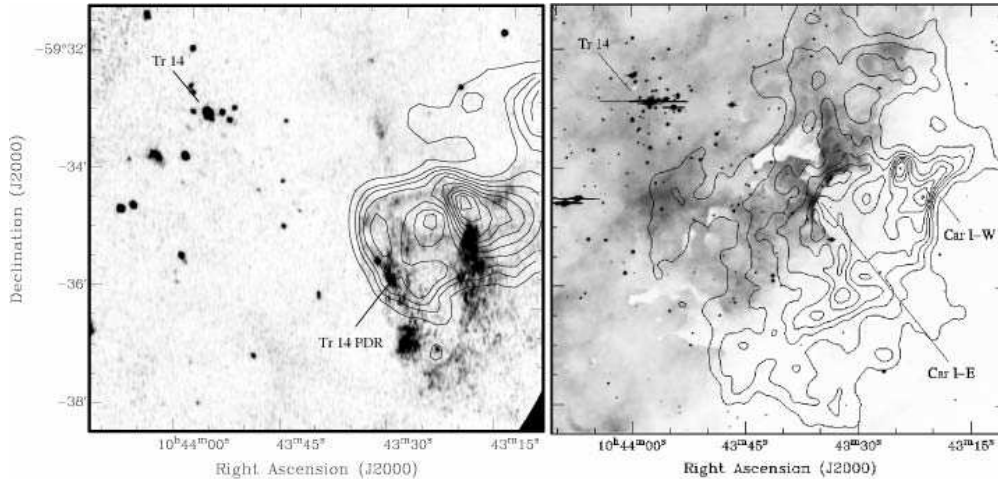


Figure 11. The edge-on PDR near Tr 14. *Left*: $^{13}\text{CO}(2-1)$ contours (Brooks et al. 2003) on $3.3\ \mu\text{m}$ PAH emission (Rathborne et al. 2002). *Right*: 4.8 GHz radio continuum contours (Brooks et al. 2001) on an $\text{H}\alpha$ image.

6. Main Regions of Interest II: The Edge-On PDR Near Tr 14

From the distribution of molecular gas shown in Figure 9 it is evident that the molecular cloud in the vicinity of Tr 14 is more intact than the remaining fragments in the Keyhole. In this so-called northern molecular cloud, the brightest molecular emission is concentrated toward the dark western dust lane seen in visual images, offset from the center of Tr 14 by $\sim 4'$. The radio continuum emission source Car I is also located here, centered on the interface of the dust lane and the bright H II region. Between Car I and the molecular cloud, widespread PDR emission is seen in arc-like PAH emission features at $3.3\ \mu\text{m}$ (Rathborne et al. 2002). The spatial sequence of Tr 14, Car I, PAH emission, and then strong molecular-line emission delineates a classical edge-on PDR (Brooks et al. 2003).

Figure 11 shows the spatial relationship of Tr 14, the ionized gas, the PDR emission, the molecular gas, and the dark dust lane. The curved edges of both ^{13}CO and $3.3\ \mu\text{m}$ PAH emission correspond to a bright optical rim at the edge of the dark lane in $\text{H}\alpha$, and match a curved radio continuum arc identified as Car I-E (see Fig. 11). There is a clear detection of the CS(5-4) line here, which indicates the presence of high density gas (Brooks et al. 2003), near the critical H_2 density of $n_{cr}(\text{H}_2) = 8 \times 10^6\ \text{cm}^{-3}$ for this transition. Curving in the same direction but located at the western edge of the continuum emission is a second arc, labeled Car I-W. Its sharp edge marks a western boundary of the extended radio continuum. Two compact H II regions have also been identified with fluxes that correspond to ionization by single O9.5 and B0-type stars, which may trace recent star-forming activity in the northern cloud. Tapia et al. (2006, 2003) have also identified potential sites of ongoing star formation here.

The northern molecular cloud appears to wrap around Car I, suggesting that Tr 14 may be carving out a small ionized cavity. $\text{H}110\alpha$ recombination-line data do not exhibit the characteristic double-peaked profiles of expansion, but if the expansion velocity is smaller than the sound speed of the ionized gas, the profiles of Car I would be consistent with an age $< 10^6$ yr (Brooks et al. 2003).

To study the properties of the PDR at the interface of the dust lane, Brooks et al. (2003) utilized observations of the fine-structure emission lines [C II] 158 μm and O I 63 μm from the Kuiper Airborne Observatory (KAO), as well as 43 – 196 μm data from the Long Wavelength Spectrometer (LWS) onboard ISO. Strong [C II] 158 μm and [O I] 63 μm emission is concentrated toward the dark dust lane, in good correspondence with the molecular gas. Results from a 1-dimensional PDR model toward the [C II] 158 μm emission peak imply a density of 10^4 cm^{-3} and a FUV field of $10^4 G_0$, where $G_0 = 1.6 \times 10^{-3} \text{ ergs s}^{-1} \text{ cm}^{-2}$ is the Habing flux (Habing 1968), representing the average diffuse FUV flux of the local interstellar radiation field. Using the ISO spectrum, estimates of the dust temperatures were found to be 40 – 50 K towards the PDR and the molecular cloud and 65 K toward the H II region. Such a temperature gradient was first noted by Cox (1995) using high-resolution images of the Carina Nebula in the four IRAS bands. The clear tendency for the IR distribution to shift away from Tr 14 as one goes from the mid-IR to far-IR signifies a strong temperature gradient, likely caused by external heating from the massive stars in Tr 14.

At a projected distance of ~ 2 pc, the UV output of Tr 14 dominates over the other Carina Nebula clusters like Tr 16 in determining the local FUV flux at the PDR in the northern cloud (Brooks et al. 2003; Smith 2006a). The emanating radiation field is sufficient to produce the ionization fronts and the FUV flux measured at the PDR emission peak. Furthermore, the kinetic energy provided by the stellar winds can sustain the high velocity dispersion measured in the molecular gas (Brooks et al. 2003). A value of $\sim 10^4 G_0$ from the Tr 14 FUV field is comparable to that found in 30 Dor, but weaker than the $\sim 10^5 G_0$ fields in regions such as M17, the Orion Bar, and W49N. In Orion, the characteristics of the O6-O7 star $\theta^1\text{Ori C}$ determine most of the properties of the ionized material and the PDR (O’Dell 2001; Hollenbach & Tielens 1997). The distance between $\theta^1\text{Ori C}$ and the main ionization front is ~ 0.25 pc, while the distance between Tr 14 and Car I is ~ 2 pc. Moreover, the ionization front adjacent to the brightest [C II] emission in 30 Dor is located ~ 20 pc from the luminous cluster R136 (Israel et al. 1996). Thus, the greater displacement between the ionization fronts and the exciting clusters in Tr 14 and 30 Dor explains why the measured PDR FUV fields are lower. Evidently, Tr 14 has been more effective or has had more time to clear away its immediate birth environment (Tr 14 is probably 1–2 Myr old, while $\theta^1\text{Ori C}$ in the Trapezium is only of order 0.1–1 Myr old).

7. Main Regions of Interest III: Star Formation in the South Pillars

In the past few years, it has become clear that the most active region of ongoing star formation in the Carina Nebula is the so-called “South Pillars”, where winds and UV radiation from Tr 14 and 16 are sweeping through and destroying a GMC. From a census of the stellar energy budget in the region (Smith 2006a), the FUV field in the south pillars is milder than in the central parts of the nebula; it falls in the range of roughly 500–5000 G_0 . The significance of this region was first recognized after wide field thermal-IR images from the *MSX* satellite became available (Smith et al. 2000; see Fig. 8b), changing the predominant view that Carina was an evolved H II region without active star formation. Since then, it has become the main focus for studies investigating ongoing and triggered star formation in Carina. A recent Spitzer/IRAC image of the South Pillars is shown in Figure 12. It is clear from this image that there

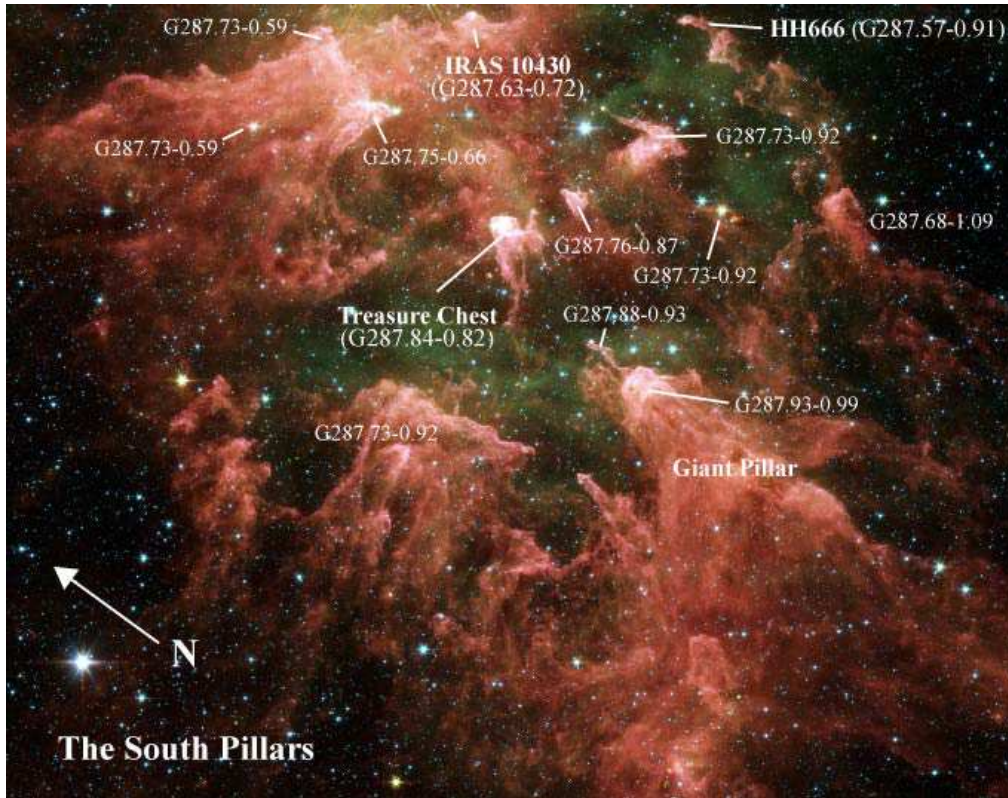


Figure 12. Spitzer/IRAC image of the South Pillars (Smith et al., in prep).

are many interesting sites of ongoing star formation in addition to the few case studies described below, which are so far the ones that have been examined in detail.

- *IRAS 10430-5931*: A study of this embedded IR source by Megeath et al. (1996) provided the first strong evidence that active star formation was still happening in the Carina Nebula. This source is embedded in a bright-rimmed globule at the inner edge of the dark obscuring dust lane that bisects the Carina Nebula, and points toward η Car (see Fig. 12). Megeath et al. estimated that this globule has a luminosity of roughly $10^4 L_{\odot}$ with $\sim 70 M_{\odot}$ of gas, possibly containing several embedded point sources. The recognition that this was a site of active star formation at the edge of the molecular cloud south of η Car suggested that astronomers needed to be looking farther away from the core of the nebula to the south and southeast in order to identify additional sites of star formation. This work has just begun, and a few such sources are identified below.

- *HH 666 - The Axis of Evil*: One definite signpost of active star formation is the presence of protostellar outflows, or Herbig-Haro jets, that punch out of a molecular cloud core where young embedded stars are actively accreting material from their circumstellar disk. The first protostellar outflow to be identified in Carina is HH 666, dubbed the “Axis of Evil” (Smith et al. 2004a). This is a remarkably straight, several parsec-long bipolar jet (see Fig. 13) emanating from a molecular globule G287.57-0.91 in the South Pillar region. In the near-IR, the jet exhibits extremely bright [Fe II] emission, but is

Table 3. Embedded star formation sites in Carina

Source	α_{2000}	δ_{2000}	Other name
G287.22-0.53	10 42 49.2	-59 25 27	...
G287.57-0.91	10 43 51.3	-59 55 22	HH 666
G287.68-1.09	10 43 57.2	-60 08 25	...
G287.87-1.36	10 44 17.9	-60 27 46	IRAS 10423-6011
G287.47-0.54	10 44 32.8	-59 33 20	N4
G287.73-1.01	10 44 34.6	-60 05 36	HD 93222
G287.73-0.92	10 44 45.4	-59 59 16	...
G287.51-0.49	10 44 59.0	-59 31 24	...
G287.63-0.72	10 45 01.1	-59 47 06	IRAS 10430-5931
G287.52-0.41	10 45 20.9	-59 27 28	IRAS 10434-5911
G287.76-0.87	10 45 22.3	-59 58 23	...
G287.84-0.82	10 45 53.6	-59 57 10	Treasure Chest
G287.93-0.99	10 45 56.1	-60 08 50	Giant Pillar
G287.88-0.93	10 46 00.9	-60 05 12	IRAS 10441-5949
G287.75-0.66	10 46 01.2	-59 46 58	...
G287.73-0.59	10 46 08.0	-59 42 41	...
G287.86-0.82	10 46 13.9	-59 58 41	...
G287.80-0.56	10 46 46.8	-59 43 25	...
G288.07-0.80	10 47 35.4	-60 02 51	...

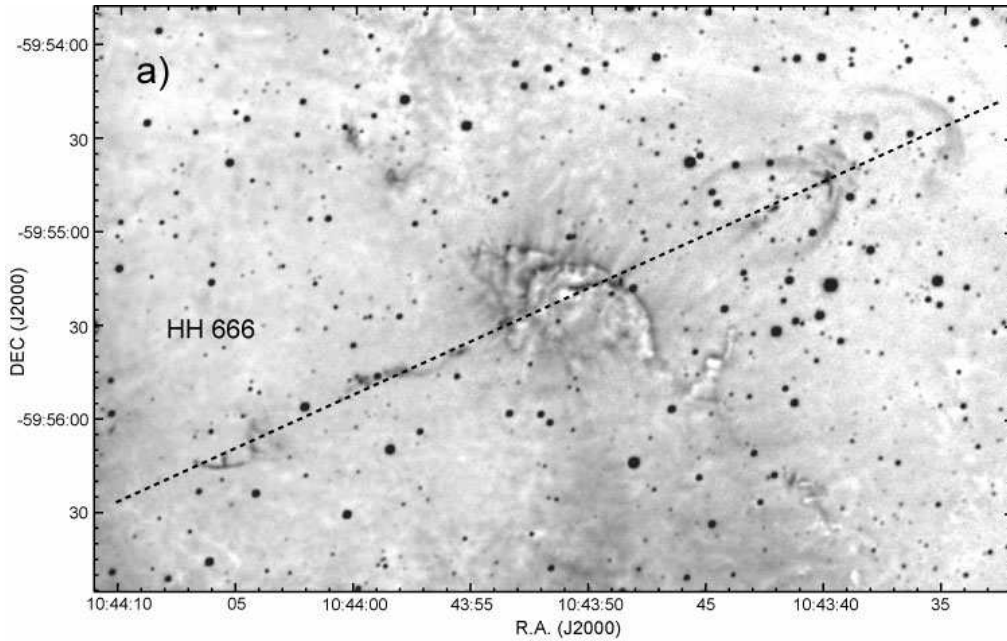


Figure 13. The Axis of Evil in the Carina Nebula. HH 666 is the first Herbig-Haro jet to be identified here (from Smith et al. 2004a).

not seen in H_2 . The embedded source is likely to be an intermediate-luminosity ($\sim 200 L_{\odot}$) Class I protostar called HH 666 IRS, located at $10^{\text{h}}43^{\text{m}}51^{\text{s}}.3, -59^{\circ}55'21''$ (J2000). This jet was identified on ground-based images, and was seen because it is the most spectacular jet in the region, and one of the longest HH jets known to date. It is likely that many other HH jets are still waiting to be discovered in Carina (see preliminary results from HST below).

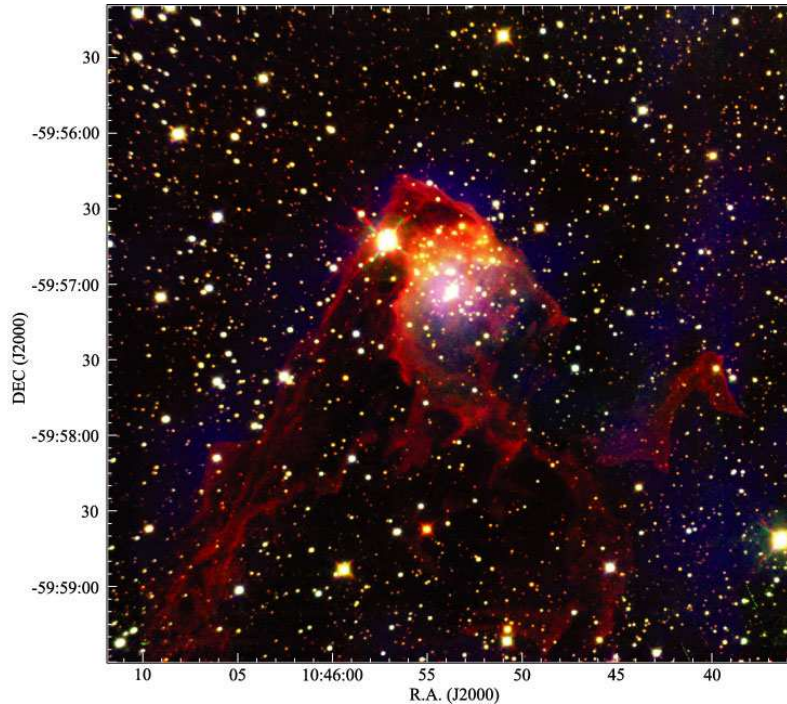


Figure 14. Narrowband near-IR image of the Treasure Chest, an embedded cluster in the South Pillar region. Blue is $\text{Pa}\beta$, green is $[\text{Fe II}] \lambda 16435$, and red is H_2 (see Smith et al. 2005).

- *The Treasure Chest:* In addition to individual young stars embedded within the heads of dust pillars, the South Pillar region also contains young embedded clusters. The brightest and most spectacular of these (and the only one yet to be studied in detail) is the Treasure Chest cluster associated with the dust pillar G287.84-0.82 (Smith et al. 2005; Hägele et al. 2004; Rathborne et al. 2004). A narrowband near-IR image of the Treasure Chest is shown in Figure 14, where the young star cluster is seen to be carving out a cavity inside the head of a dust pillar, the outside of which has a bright and spectacular PDR seen in H_2 emission. The most luminous member of this star cluster is the O9.5 V star CPD- $59^{\circ}2661$. It can be seen at optical wavelengths, surrounded by a small fuzzy H II region that has been known for some time (Thackeray 1950b; Walsh 1984). Smith et al. (2005b) found that this embedded cluster (with A_V as high as 50) was very young, with a likely age less than 0.1 Myr. They also found that it has one of the highest disk fractions of any known embedded cluster; the disk fraction is 67% measured from near-IR excess in the K band. Higher disk fractions generally result when longer-wavelength data are included. For example, the young cluster NGC 2024 has a disk fraction of 60% measured in JHK photometry (lower than Carina's Treasure

Chest), but a higher disk fraction of 90% when L-band photometry is included (Haisch et al. 2000). Thus, the true disk fraction in Carina's Treasure Chest may be near 100%, making it a valuable target for learning about the effect of UV irradiation from nearby O stars on young protoplanetary disks.

- *The Giant Pillar:* Among the South Pillars, the largest one is a giant dust pillar more than 25 pc across that points toward η Carinae (Smith et al. 2000). Many smaller dust pillars, more typical of those seen in other H II regions, are seen to sprout from this one giant pillar, which also contains several embedded IR sources (Fig. 12; Rathborne et al. 2004). This giant pillar is probably the remains of a GMC core that is being shredded by feedback from the stars in Tr 16. This and several additional pillars in this region await detailed study.

In addition to these, there are many other sites of ongoing star formation in the South Pillars region and around the Carina Nebula (see Figures 8a and 12). A list of several mid-IR sources with embedded stars is given in Table 3, compiled from Rathborne et al. (2004) and Smith et al. (2000). Some of these are potentially sites of embedded, ongoing *massive* star formation.

8. A Preview of Coming Attractions

8.1. An HST/ACS H α Survey of Carina

At the time of writing this review, the first large imaging survey of the Carina Nebula with the Hubble Space Telescope (HST) has just been completed, and so far the results are stunning. The only previous HST imaging of Carina involved smaller WFPC2 fields of view centered on η Carinae, part of the Keyhole Nebula, and Tr 14. The new contiguous mosaic image of the bright region of the nebula was obtained with the ACS/WFC camera using the H α (F658N) filter. It has been released as a stunning color image as part of the Hubble Heritage project¹, the main part of which is shown in Figure 15.

The huge HST mosaic image is one of the largest made by HST, and contains an enormous amount of detail. A small taste of the imminent results can be seen in Figure 16, which displays just a small few arcminute-wide section of the nebula. Here we see a dust pillar just north of the Tr 14 cluster which is being eroded by stellar winds. The zoomed-in view shows two spectacular bipolar Herbig-Haro jets, HH 901 and 902, emerging from near the tips of two smaller dust pillars. Several other HH jets are seen in the HST data as well. In addition to the first HH jet to be discovered in Carina (HH 666; Smith et al. 2004a) these HH jets are signposts of active ongoing star formation still embedded within the dust pillars that are now being demolished.

The new HST data provide an immensely complex and large dataset, and are unfortunately still in the early stages of analysis, so we cannot provide a summary of the results (such as a Table of all the HH jets discovered), but combined with data from Spitzer, we expect them to shed important new light on the outflow activity and the embedded stellar population in Carina. Such papers are currently in preparation (Smith et al.).

¹<http://heritage.stsci.edu/2007/16/index.html>



Figure 15. The recent HST/ACS- $H\alpha$ imaging survey of the Carina Nebula (PI: Smith), from a mosaic released by the Hubble Heritage Team. The color map is taken from ground based images in the usual filters with [O III]=blue, $H\alpha$ =green, and [S II]=red. η Car is at the very bottom. *Image credit:* N. Smith, NASA, ESA.

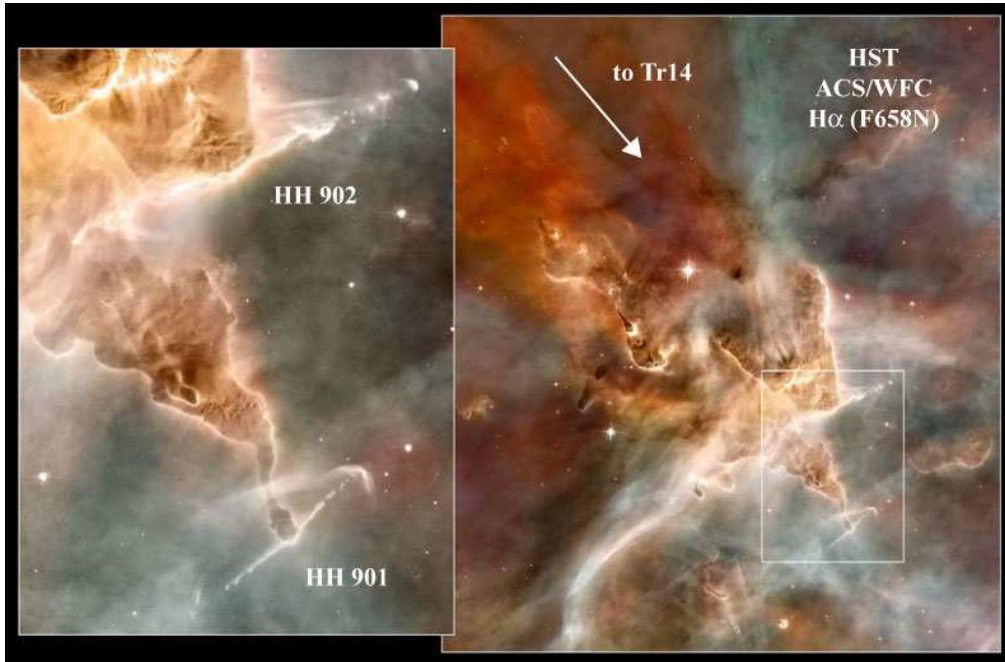


Figure 16. One small section of the HST images in the previous figure. This detail shows a region about $10'$ north of the Tr 14 cluster, containing a dust pillar in the process of being shredded. Two newly discovered bipolar Herbig-Haro jets, HH 901 and 902, emerge from Class I protostars buried within the heads of the dust pillars (Smith et al. in prep.).

8.2. Recent and Planned X-ray Observations with *XMM* and *Chandra*

The diffuse X-ray emission in the Carina Nebula is unusually luminous, about 10-100 times stronger than other giant H II regions, and it was the first among giant H II regions to be discovered to have diffuse X-rays (Seward et al. 1979; Seward & Chlebowski 1982). Not surprisingly then, it is an important target for the currently-available suite of X-ray telescopes in space such as *XMM-Newton*, the *Chandra* X-ray Observatory, and the *Suzaku* (Astro-E2) mission.

Figure 17 shows a wide-field mosaic image of the diffuse X-ray emission in Carina (K. Hamaguchi, private comm.), composed of several individual pointings taken with the *XMM-Newton* satellite. It illustrates that the emission from Carina is a complex combination of point sources from O stars, WNH stars, and colliding wind binaries, plus diffuse soft X-ray emission that spans more than 1° . Many of the point sources are fascinating systems in their own right (many are colliding-wind binaries like η Car and WR25; see Corcoran 2005, Raassen et al. 2003), but we will not review the X-ray properties of these massive stars here. Some fraction of the diffuse emission may also be contributed by unresolved low-mass T Tauri stars that have formed alongside the massive members of these clusters and throughout the nebula, so spatial resolution is an issue when interpreting the data. With the superior spatial resolution of *Chandra*, preliminary studies of small regions around Tr 16 and Tr 14 have revealed hundreds of point sources (Evans et al. 2003; Townsley 2006; Sanchawala et al. 2007), but so far only a portion of the inner nebula has been studied with *Chandra*. An accurate

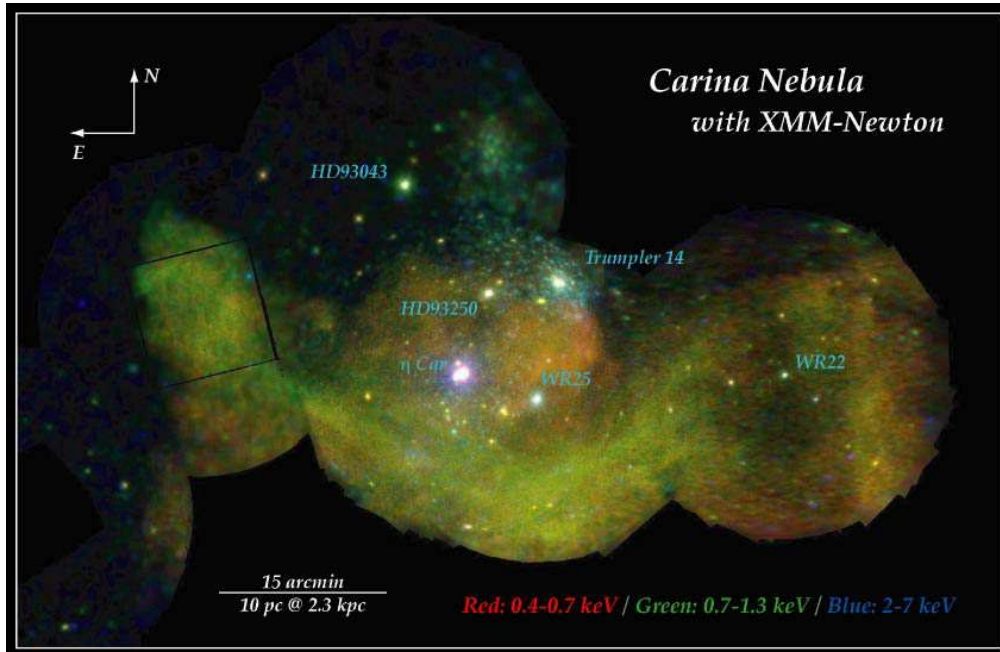


Figure 17. Wide-field X-ray image of the inner Carina Nebula taken with XMM. Soft X-rays (0.4-0.7 keV) are in red, medium/soft X-rays (0.7-1.3 keV) are in green, and harder X-rays are in blue. Several key sources are identified. *Image credit:* K. Hamaguchi, NASA, ESA

census of the low-mass X-ray emitting stellar population will be an important goal of an upcoming large survey of Carina with Chandra (PI: L. Townsley).

For the time being, one of the most pressing questions regarding X-ray observations of Carina is the physical origin of the unusually bright diffuse X-ray emission. The first explanation that usually comes to mind is that there may have been a recent supernova explosion in Carina. If that were true, it would have stunning implications from the point of view of stellar evolution. Namely, if a star exploded in the vicinity of Tr 16 and Tr 14, we might expect that this progenitor star had an initial mass larger than that of η Carinae because it reached the end of its life sooner. Little is known about the end fates of stars that massive, and it might alter our interpretation of η Car's role in the history of the Carina region. It would also mean that Carina is an example of a star-forming region caught in the act of polluting protostellar disks with supernova ejecta, with far-reaching implications for the origin of our own Solar System (e.g., Tachibana & Huss 2003; Hester et al. 2004; Desch & Ouellete 2005). Thus, alternatives should be considered carefully.

The diffuse emission cannot be accounted for fully by an extrapolation of the discrete source luminosity function, but on the other hand, Seward & Chlebowsky (1982) argued that energy input to the diffuse plasma from collisions of the many O-star and WNH-star winds with the ambient medium was sufficient (see also Townsley et al. 2003; Ezoe et al. 2006). Smith (2006a) also showed that the integrated mechanical energy input from stellar winds was more than enough to power the expansion of the region (see also Smith & Brooks 2007).

Thus, there appears to be no *need* to invoke a recent supernova explosion on energetic grounds alone, but there are some other clues that make the specter of a supernova a hard hypothesis to rule out. For instance, the spectral energy distribution of the diffuse X-ray emission in Carina varies with position in a peculiar way. Studies of the diffuse emission with XMM-Newton, Chandra, and Suzaku (Hamaguchi et al. 2007; Townsley 2006) show that the diffuse emission immediately south of Tr 14 and north of WR25 (reddish hue in Fig. 17) has both an intermediate/hard component at 0.62 keV and a softer component at 0.26 keV, with relatively normal abundances. By contrast the emission further south (greenish hue running east/west across the nebula in Fig. 17) requires only the 0.6 keV component (no softer X-rays) and seems to show enhanced Ne and Fe abundances. Hamaguchi et al. (2007) suggest that the lack of strong nitrogen enrichment and normal oxygen abundances favor the SN hypothesis, because one would expect stellar winds to contribute more nitrogen rich material. However, Smith & Morse (2004) showed that even in the case of an evolved massive star like η Car, the N-rich ejecta are tightly confined to within about $1'$ of the star, with progressively more normal N/O ratios at larger radii from the star. Also, examining the different color of X-ray emission in Figure 17 that represents different energies, one might wonder why the plasma that lacks a soft component and has enhanced Fe and Ne abundances (green) is spatially coincident with the V-shaped dust lane that bisects the nebula (see Fig. 8). This region has the highest line-of-sight column density in the nebula (Smith & Brooks 2007), so it is not clear how strong absorption through a clumpy medium might affect the spectra. The alternative that a supernova focussed Fe-rich ejecta exclusively toward the dust lane seems dubious. These questions do not appear to have easy solutions with available data.

Overall, we still do not know the origin of the diffuse X-ray emission in Carina, and we look forward with great anticipation to the results of the upcoming large survey with Chandra.

9. Closing Remarks

In this review, we have highlighted recent work that portrays the Carina Nebula as a rich star-forming region, and a laboratory in which to study feedback from massive stars. It gives examples of the same detailed phenomena seen in closer regions like Orion, while sampling a much more extreme stellar population analogous to that of 30 Dor. The vicinity of the Keyhole Nebula gives us a view of the remnant of a GMC that has already been dispersed by massive stars in Tr 16, while the northern cloud near the younger Tr 14 cluster is more intact, still awaiting vigorous star formation. The South Pillars currently harbor the most active star formation in Carina, where stellar winds and radiation are sculpting dust pillars and probably triggering a new generation of stars.

Despite these recent highlights, we suspect that the most exciting work on Carina remains to be done, with more comprehensive study of the overall properties of the gas and embedded stars. Recent surveys with *HST*, *Spitzer*, and *Chandra* will soon yield a rich harvest of new results. The brightness and complexity of Carina will undoubtedly provide new discoveries and exciting new challenges for future IR observatories like SOFIA and Herschel, and it will no-doubt be a bonanza for planned millimeter projects in the southern hemisphere like ALMA and the single-dish telescopes at the same site.

Acknowledgements. We thank Nolan Walborn for helpful comments after a careful reading of this manuscript as the referee, as well as D. Malin, J. Rathborne, and Y. Yonekura for use of their data. We also thank the ATNF Distinguished Visitor Program, providing us with an opportunity to collaborate on this review in person in Australia. N.S. was supported by NASA through grants GO-10241 and GO-10475 from STScI.

References

- Allen, D.A. 1979, MNRAS, 189, 1
 Allen, D.A. & Hillier, D.J. 1993, PASA, 10, 338
 Ascenso, J., Alves, J., Vicente, S., & Lago, M.T.V.T. 2007, A&A, 976, 199
 Blaauw, A. 1964, ARAA, 2, 213
 Bok, B.J. 1932, Harvard Reprints, 1, 77
 Brooks, K.J., Burton, M.G., Rathborne, J.M. et al. 2000, MNRAS, 319, 95
 Brooks, K.J., Cox, P., Schneider, N., et al., 2003, A&A, 412, 751
 Brooks, K.J., Garay, G., Nielbock, M., Smith, N., & Cox P. 2005, ApJ, 634, 436
 Brooks, K.J., Storey, J.W.V., & Whiteoak, J.B. 2001, MNRAS, 327, 46
 Brooks, K.J., Whiteoak, J.B., & Storey, J.W.V. 1998, Pub. Astron. Soc. Australia, 15(2), 202
 Carraro, G. 2002, MNRAS, 331, 785
 Carraro, G. & Patat, F. 2001, A&A, 379, 136
 Carraro, G., Patat, F., & Baumgardt, H. 2001, A&A, 371, 107
 Carraro, G., Romaniello, M., Ventura, P., & Patat, F. 2004, A&A, 418, 525
 Caswell, J.L. 1998, MNRAS, 297, 215
 Caswell, J.L. & Haynes, R.F. 1975, MNRAS, 173, 649
 Cersosimo, J.C., Azcarate, I.N., & Colomb, F.R. 1984, ApJ, 24, 1
 Chan, K.W. & Onaka, T. 2000, ApJ, 533, L33
 Corcoran, M.F. 2005, AJ, 129, 2018
 Cox, P. 1995, Rev. Mex. Astron. Astrofis. Ser. Conf., 2, 105
 Cox, P. & Bronfman, L. 1995, A&A, 299, 583
 Crowther, P.A., Smith, L.J., Hillier, D.J., & Schmutz, W. 1995, A&A, 293, 427
 Davidson, K., & Humphreys, R.M. 1997, ARA&A, 35, 1
 Daminieli, A., Kaufer, A., Wolf, B. et al. 2000, ApJ, 528, L101
 de Graauw, T., Lidholm, S., Fitton, B., et al. 1981, A&A, 102, 257
 DeGioia-Eastwood, K., Throop, H., Walker, G., & Cudworth, K.M. 2001, ApJ, 549, 578
 Deharveng, L. & Maucherat, M. 1975, A&A, 41, 27
 Desch, S.J. & Ouellete, N. 2005, Lunar Planet Sci. Conf., 36, 1327
 Dickel, H.R. 1974, A&A, 31, 11
 Dickel, H.R. & Wall, J.V. 1974, A&A, 31, 5
 Elliot, K.H. 1979, MNRAS, 186, 9
 Evans, N.R., Seward, F.D., Krauss, M.I. et al. 2003, ApJ, 589, 509
 Ezoe, Y., Kokubun, M., Makishima, K. et al. 2006, ApJ, 638, 860
 Feinstein, A. 1982, AJ, 87, 1012
 Feinstein, A. 1995, RevMexAA, Ser. Conf., 2, 57
 Feinstein, A. & Marraco, H. G. 1980, PASP, 92, 266
 Feinstein, A., Marraco, H. G., & Muzzio, J. C. 1973, A&AS, 12, 331
 Feinstein, A., Moffat, A.F.J., & Fitzgerald, M.P. 1980, AJ, 85, 708
 Figer, D.F., Kim, S.S., Morris, M. et al. 1999, ApJ, 525, 750
 Figer, D.F., Najarro, F., Gilmore, D. et al. 2002, ApJ, 581, 258
 Fitzgerald, M.P. & Mehta, S. 1987, MNRAS, 228, 545
 Forte, J.C. 1978, AJ, 83, 1199
 Frew, D.J. 2004, J. of Astron. Data, 10, 6
 Gaensler, B.M., McClure-Griffiths, N.M., Oey, M.S., Haverkorn, M., Dickey, J.M., & Green, A.J. 2005, ApJ, 620, L95

- Garcia, B. & Walborn, N.R. 2000, *PASP*, 112, 1549
- Garcia, B., Malaroda, S., Levato, H., Morrell, N., & Grosso, M. 1998, *PASP*, 110, 53
- Gardner, F.F., Dickel, H.R., & Whiteoak, J.B. 1973, *A&A*, 23, 51
- Gardner, F.F. & Morimoto, M. 1968, *Aust. J. Phys.*, 21, 881
- Gardner, F.F., Milne, D.K., Mezger, P.G., & Wilson, T.L. 1970, *A&A*, 7, 349
- Gaviola, E. 1950, *ApJ*, 111, 408
- Ghosh, S.K., Iyengar, K.V.K., Rengarajan, S.N., et al. 1988, *ApJ*, 330, 928
- Grabelsky, D.A., Cohen, R.S., Bronfman, L., & Thaddeus, P. 1988, *ApJ*, 331, 181
- Habing, H.J. 1968, *Bull. Astron. Neth.*, 19, 421
- Haisch, K.E., Lada, E.A., & Lada, C.J. 2000, *AJ*, 120, 1396
- Hägele, G.F., Albacete Colombo, J.F., Barba, R.H., & Bosch, G.L. 2004, *MNRAS*, 355, 1237
- Harvey, P.M., Hoffmann, W.F., & Campbell, M.F. 1979, *ApJ*, 227, 114
- Herbst, W. 1976, *ApJ*, 208, 923
- Herschel, J.F.W. 1847, *Results of Observations Made During the Years 1834, 5, 6, 7, 8 at the Cape of Good Hope* (London: Smith, Elder)
- Hester, J.J., Desch, S.J., Healy, K.R., & Leshin, L.A. 2004, *Science*, 304, 1116
- Hollenbach, D.J. & Tielens, A.G.G.M. 1997, *ARA&A*, 35, 179
- Huchtmeier, W.K. & Day G.A. 1975, *A&A*, 41, 153
- Humphreys, R.M. 1978, *ApJS*, 38, 309
- Israel, F.P., Maloney, P.R., Geis, N., et al. 1996, *ApJ*, 465, 738
- Jones, B.B. 1973, *Aust. J. Phys.*, 26, 545
- Kaltcheva, N.T. & Georgiev, L.N. 1993, *MNRAS*, 261, 847
- Lada, C.J. & Lada, E.A. 2003, *ARAA*, 41, 57
- Laurent, C., Paul, J.A., & Pettini, M. 1982, *ApJ*, 260, 163
- Lee, D.H., Min, K.W., Dixon, W.V.D. et al. 2000, *ApJ*, 545, 885
- Levato, H., Malaroda, S., Morrell, N., Garcia, B., & Hernandez, C. 1991, *ApJS*, 75, 869
- Lopez, J.A. & Meaburn, J. 1986, *Rev. Mex. Astron. Astrofis.*, 13, 27
- Marraco, H.G., Vega, E.I., & Vrba, F.J. 1993, *AJ*, 105, 258
- Massey, P. & Johnson, J. 1993, *AJ*, 105, 980
- Massey, P. & Hunter, D.A. 1998, *ApJ*, 493, 180
- Meaburn, J., Lopez, J.A., & Keir, D. 1984, *MNRAS*, 211, 267
- Megeath, S.T., Cox, P., Bronfman, L., & Roelfsema, P.R. 1996, *A&A*, 305, 296
- Mizutani, M., Onaka, T., & Shibai, H. 2004, *A&A*, 423, 579
- Moffat, A.F.J. & Vogt, N. 1975, *A&A*, 20, 125
- Moffat, A.F.J., Corcoran, M. F., Stevens, I.R. et al. 2002, *ApJ*, 573, 191
- Morrell, N., Garcia, B., & Levato, H. 1988, *PASP*, 100, 1431
- Najarro, F., Figer, D.F., Hillier, D.J., & Kudritzki, R.P. 2004, *ApJ*, 611, L105
- O'Dell, C. R. 2001, *ARA&A*, 39, 99
- Raassen, A.J.J., van der Hucht, K.A. Mewe, R. et al. 2003, *A&A*, 402, 653
- Rathborne, J.M., Brooks, K.J., Burton, M.G., Cohen, M., & Bontemps, S. 2004, *A&A*, 418, 563
- Rathborne, J.M., Burton, M. G., Brooks, K.J., et al. 2002, *MNRAS*, 331, 85
- Reipurth, B., Raga, A., & Heathcote, S. 2003, *AJ*, 126, 1925
- Retallack, D. S. 1983, *MNRAS*, 204, 669
- Sanchawala, K., Chen, W.P., Lee, H.T., al. 2007, *ApJ*, 656, 462
- Schwartz, R.D., Persson, S.E., & Hamann, F.W. 1990, *AJ*, 100, 793
- Seward, F.D. & Chlebowski, T. 1982, *ApJ*, 256, 530
- Seward, F.D., Forman, W.R., Giacconi, R., et al. 1979, *ApJ*, 234, L55
- Shaver, P. A. & Goss, W. M. 1970, *Australian J. Phys. Suppl.*, 14, 133
- Sher, D. 1965, *Quart. J. R. Astron. Soc.*, 6, 299
- Shobbrook, R.R. 1980, *MNRAS*, 192, 821
- Shobbrook, R.R. & Lynga, G. 1994, *MNRAS*, 269, 857
- Smith, N. 2002a, *MNRAS*, 337, 1252
- Smith, N. 2002b, *MNRAS*, 331, 7
- Smith, N. 2006a, *MNRAS*, 367, 763

- Smith, N. 2006b, ApJ, 644, 1151
 Smith, N. & Brooks, K.J. 2007, MNRAS, 379, 1279
 Smith, N. & Conti, P.S. 2008, ApJ, 679, 1467
 Smith, N. & Morse, J.A. 2004, ApJ, 605, 854
 Smith, N., Egan, M.P., Carey, S., et al. 2000, ApJ, 532, L145
 Smith, N., Bally, J., & Morse, J.A. 2003a, ApJ, 587, L105
 Smith, N., Gehrz, R.D., Hinz, P.M. et al. 2003b, AJ, 125, 1458
 Smith, N., Bally, J., & Brooks, K.J. 2004a, AJ, 127, 2793
 Smith, N., Barba, R.H., & Walborn, N.R. 2004b, MNRAS, 351, 1457
 Smith, N., Morse, J.A., & Bally, J. 2005a, AJ, 130, 1778
 Smith, N., Stassun, K.G., & Bally, J. 2005b, AJ, 129, 888
 Smith, N., Bally, J., & Walawender, J. 2007, AJ, 134, 846
 Smith, R.G. 1987, MNRAS, 227, 943
 Tachibana, S. & Huss, G.R. 2004, ApJ, 588, L41
 Tapia, M., Roth, M., Marraco, H., & Ruiz, M.T.. 1988, MNRAS, 232, 661
 Tapia, M. 1995, Rev. Mex. Astron. Astrofis. Ser. Conf., 2, 87
 Tapia, M., Roth, M., Vazquez, R.A., & Feinstein A. 2003, MNRAS, 339, 44
 Tapia, M. 2004, Rev. Mex. Astron. Astrofis. Ser. Conf., 22, 73
 Tapia, M., Persi, P., Bohigas, J., Roth, M., & Gomez, M. 2006, MNRAS, 367, 513
 Tateyama, C.E., Strauss, F.M., & Kaufmann, P. 1991, MNRAS, 249, 716
 Thackeray, A.D. 1950a, 110, 529
 Thackeray, A.D. 1950b, MNRAS, 110, 524
 Thé, P.S., Bakker, R., & Tjin A Djie, H.R.E. 1980, A&A, 89, 209
 Thé, P.S. & Vleeming, G. 1971, A&A, 14, 120
 Townsley, L.K. 2006, in Proc. STScI May Symposium, *Massive stars: From PopIII and GRBs to the Milky Way*, ed. M. Livio (astro-ph/0608173)
 Townsley, L.K., Feigelson, E.D., Montmerle, T., Broos, P.S., Chu, Y.H., & Garmire, G.P. 2003, ApJ, 593, 874
 Turner, D.G., Grieve, G.R., Herbst, W., & Harris, W.E. 1980, AJ, 85, 1193
 Vazquez, R.A., Baume, G., Feinstein, A., & Prado, P. 1996, A&AS, 116, 75
 Walborn, N.R. 1973, ApJ, 179, 517
 Walborn, N.R. 1975, ApJ, 202, L129
 Walborn, N.R. 1982, ApJS, 48, 145
 Walborn, N.R. 1995, Rev. Mex. Astron. Astrofis. Ser. Conf., 2, 51
 Walborn, N.R. 2002, ASP Conf. Ser. 267, *Hot Star Workshop III: The Earliest Stages of Massive Star Birth*, ed. P.A. Crowther (San Francisco: ASP), 111
 Walborn, N.R. & Hesser, J.E. 1975, ApJ, 199, 535
 Walborn, N.R. & Hesser, J.E. 1982, ApJ, 252, 156
 Walborn, N.R. & Liller, M.H. 1977, ApJ, 211, 181
 Walborn, N.R., Danks, A.C., Vieira, G., & Landsman, W.B., 2002a, ApJS, 140, 407
 Walborn, N.R., Howarth, I.D., Lennon, D.J. et al. 2002b, AJ, 123, 2754
 Walborn, N.R., Smith, N., Howarth, I.D., Vieira, G. et al. 2007, PASP, 119, 156
 Walsh, J.R. 1984, A&A, 138, 380
 Welch, W.J., Dreher, J.W., Jackson, J.M. et al. 1987, Science, 238, 1550
 Whiteoak J.B. & Otrupcek R.E. 1984, PASA, 5(4), 552
 Whiteoak J.B.Z. 1994, ApJ, 429, 225
 Whitney, B., Indebetouw, R., babler, B.L. et al. 2004, ApJS, 154, 315
 Yonekura Y., Asayama S., Kimura K. et al. 2005, ApJ, 634, 476
 Zhang X., Lee Y., Bolatto A., & Stark A.A. 2001, ApJ, 553, 274